frontiers | Frontiers in Electronic Materials

REVIEW
published: 04 May 2022
doi: 10.3389/femat.2022.891983

Recent Progress and Prospects on Metal Halide Perovskite Nanocrystals as Color Converters in the Fabrication of White Light-Emitting Diodes

*Ashutosh Mohapatra, Manav R. Kar and Saikat Bhaumik**

Department of Engineering and Materials Physics, Institute of Chemical Technology-IndianOil Odisha Campus, Bhubaneswar, India

Recently, metal-halide perovskite nanocrystals (NCs) have shown major development and have attracted substantial interest in a wide range of applications, such as light-emitting diodes (LEDs), solar cells, lasers, and photodetectors due to their attractive properties, such as superior PL emission, a wider range of color tunability, narrow emission spectra, better color purity, low cost, easy solution-processability, and so on. In the past, many color-converting materials, such as III-nitrides, organics, polymers, metal chalcogenides, were investigated for solid-state lighting (SSL) white light-emitting diodes (WLEDs). Still, they suffer from issues such as low stability, low color rendering index (CRI), high correlated color temperature (CCT), low luminous efficiency (LE), and high cost. In this sense, metal-halide perovskite NCs exhibit a better color gamut compared with conventional lighting sources, and production costs are comparatively cheaper. Such materials may offer an upcoming substitute for future color-converting WLEDs. In this review, we discuss the metal halide perovskite NCs and their synthesis protocols. Then we elaborate on the recent progress of halide perovskite NCs as a conversion layer in the application of WLEDs.

Keywords: metal halide perovskite nanocrystals, color converters, white light-emitting diodes, color quality, efficiency

OPEN ACCESS

Edited by:
Wei You,
University of North Carolina at Chapel Hill, United States

Reviewed by:
Giuseppe Maria Paternò,
Politecnico di Milano, Italy
Zhiwen Jin,
Lanzhou University, China

****Correspondence:***
Saikat Bhaumik
s.bhaumik@iocb.ictmumbai.edu.in

Specialty section:
This article was submitted to Optoelectronic Materials, a section of the journal Frontiers in Electronic Materials

Received: *08 March 2022*
Accepted: *04 April 2022*
Published: *04 May 2022*

Citation:
Mohapatra A, Kar MR and Bhaumik S (2022) Recent Progress and Prospects on Metal Halide Perovskite Nanocrystals as Color Converters in the Fabrication of White Light-Emitting Diodes. Front. Electron. Mater. 2:891983. doi: 10.3389/femat.2022.891983

INTRODUCTION

Solid-state lighting (SSL) is a promising lighting technology where solid-state materials are being used as light sources (Schubert and Kim, 2005; Krames et al., 2007; D'Andrade and Forrest, 2004; Wang et al., 2018a; Dai et al., 2010; Wood and Bulović, 2010). In 1993–1994, Shuji Nakamura first introduced double-heterostructure InGaN/GaN and InGaN/AlGaN as active materials for blue LED chips that were proved to be suitable for commercial applications (Nakamura et al., 1993; Nakamura et al., 1994a; Nakamura et al., 1994b). Since then, major progress has been accomplished in the evolution of III-nitride LEDs (NLEDs), organic LEDs (OLEDs), polymer LEDs, and metal chalcogenide quantum dot LEDs (QDLEDs) (Schubert and Kim, 2005; Krames et al., 2007; D'Andrade and Forrest, 2004; Wang et al., 2018a; Dai et al., 2010; Wood and Bulović, 2010). In recent times, white light-emitting diodes (WLEDs) are very important in our daily life as they are commonly used in homes, streets, malls, TV, and displays. SSL WLEDs are much more efficient than conventional lighting sources, e.g., incandescent bulbs and fluorescence lamps, in terms of energy consumption and lead to tremendous energy saving (Tsao et al., 2010).

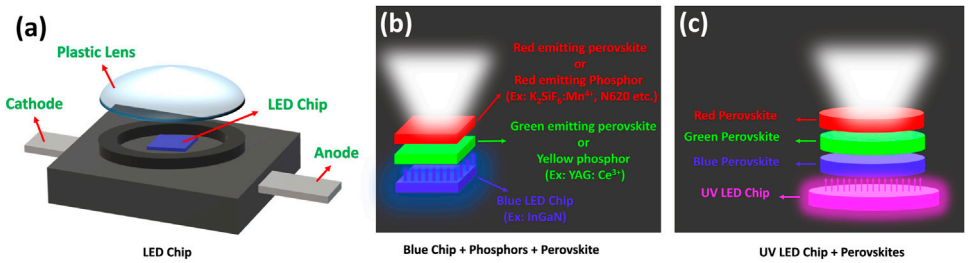

FIGURE 1 | Schematic diagrams of **(A)** a LED chip, **(B)** WLED with phosphors or perovskite materials integrated onto a blue LED chip, and **(C)** RGB color-emitting perovskite materials integrated on a UV LED chip.

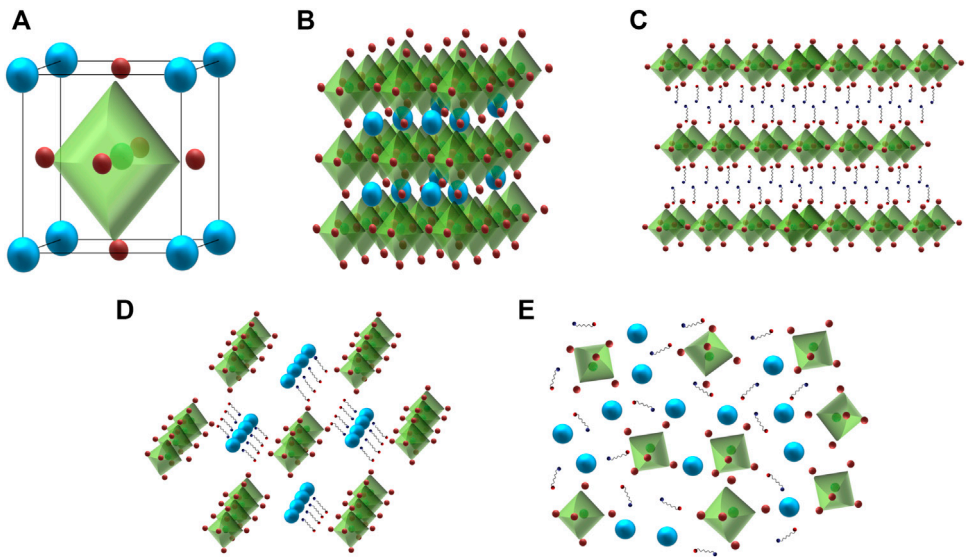

FIGURE 2 | Schematic representations of **(A)** a perovskite unit cell, **(B)** 3-D, **(C)** 2-D, **(D)** 1-D, and **(E)** 0-D metal halide perovskite structures.

The schematic diagram of a LED chip is shown in **Figure 1A**. Color-converting WLEDs are usually fabricated on a single UV or blue LED chip combined with color conversion layers (*see* **Figures 1B,C**) (Schubert and Kim, 2005; Krames et al., 2007; D'Andrade and Forrest, 2004; Wang et al., 2018a; Dai et al., 2010; Wood and Bulović, 2010). The basic operation of a WLED is based on the radiative recombination of holes and electrons produced by the injection of current into the device. The easiest method to fabricate a WLED is to embed yellow-emitting materials onto a 450- to 470-nm blue GaN LED chip. In this LED device configuration, some parts of blue light emitted from the LED chip excite the yellow-emitting materials. The residual blue light combines with the yellow light, which overall generates the white light emission. However, such WLEDs suffer from low CRI and high CCT values due to a lack of red color emission. Also, they suffer from low stability of CCT values under different driving currents (Phillips et al., 2007; Crawford, 2009; Lin et al., 2016; Baekelant et al., 2017). To improve the color quality of the WLEDs, red-green-blue (RGB) color phosphors are settled down on the top of a UV chip. These LEDs demonstrate higher device efficiency, high CRI, better chromatic stability under different driving currents (Schubert and Kim, 2005; Krames et al., 2007; D'Andrade and Forrest, 2004; Wang et al., 2018a; Dai et al., 2010; Wood and Bulović, 2010). However, the instability of CCT also happens in RGB WLEDs due to degradation of different color phosphors or variations of driving current (Phillips et al., 2007; Crawford, 2009; Baekelant et al., 2017).

Next-generation LEDs can be identified as the devices with high efficiency, high color quality, and lower economic and energy costs of manufacturing (Shirasaki et al., 2013; Dou et al., 2020). The III-nitride LEDs have transformed the conventional lighting technologies, but the preparation of these materials relies on high temperature and expensive vacuum-based processing (Mondal et al., 2021). The fabrication of OLEDs is also dependent on vacuum-based sublimation, inappropriate for cost-effective processing on large area (Sasabe and Kido, 2011). The usage of QDLEDs is restricted by large nonradiative recombination processes from the high surface-mediated defect states (Yang et al., 2019). Recently,

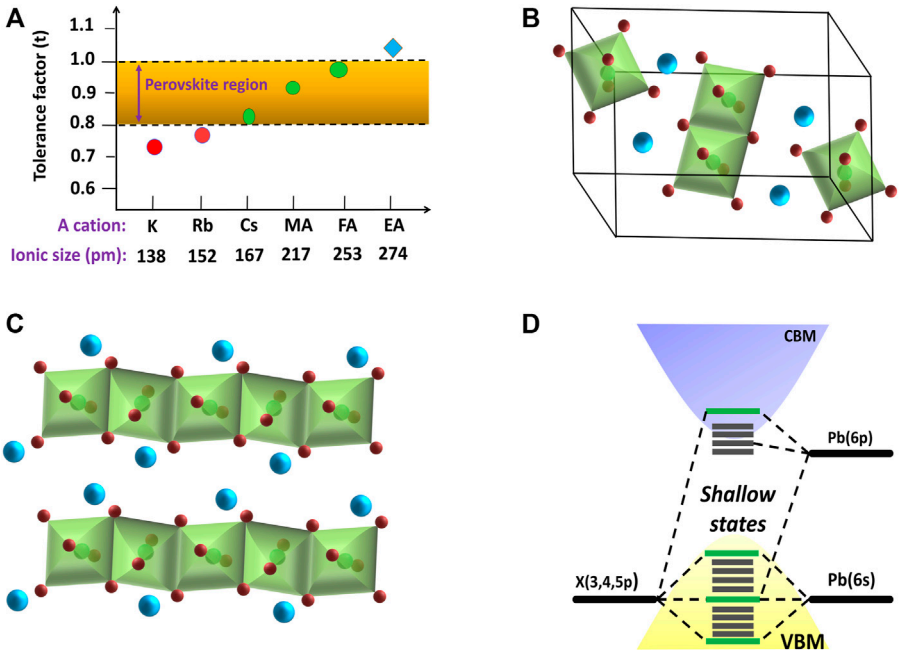

FIGURE 3 | (A) Tolerance factor of different cation-based $APbI_3$ perovskites. Schematic diagrams of yellow phase structure of **(B)** $CsPbI_3$, and **(C)** $FAPbI_3$. **(D)** Energy band structure of $APbX_3$ perovskites.

lead-halide perovskite nanocrystals (NCs) have gathered massive observations toward the fields of LEDs, solar cells, detectors, and lasing due to their tunable wavelength, high photoluminescence quantum yield (QY), narrow emission wavelength, wider color gamut, and better color purity (Kovalenko et al., 2017; Li et al., 2017; Akkerman et al., 2018; Yan et al., 2019; Zhang et al., 2019; Li et al., 2020; Li et al., 2021a). The color gamut of perovskite LEDs exceeds 140% of the National Television System Committee (NTSC) standard, surpassing the commercial OLED and QDLED displays. The high color purity, low turn-on voltage, cost-effectiveness, and low energy consumption of the perovskite NC-based LEDs make them promising candidates for next-generation display technologies. In this review, we execute our key attention toward the properties of metal halide perovskites, the synthesis of perovskite NCs, and their recent progress in WLED applications as a conversion layer.

CHARACTERISTICS OF METAL-HALIDE PEROVSKITES

Crystal Structure

Metal-halide perovskites have a distinctive crystal structure having the chemical formula in the form of AMX_3 [A: organic or inorganic cations (MA = CH_3NH_3, FA = $CH(NH_2)_2$, Cs, Rb); M: divalent metal cations (Pb, Sn); and X: halide anions (Cl, Br, I)] (Veldhuis et al., 2016; Kovalenko et al., 2017; Li et al., 2017; Akkerman et al., 2018; Yan et al., 2019; Li et al., 2020). They can be distinguished into two groups of materials depending on the type of the cations. If the A-site cation involves organic cations (i.e., MA or FA or both), then the perovskite structure belongs to the group of organometallic metal-halide perovskites. On the other hand, if the A-site cation consists of Cs, Rb-cations, then the system is considered all-inorganic metal-halide perovskites. In a three-dimensional (3-D) perovskite unit cell, the A-cations are situated at the eight corners of a $[MX_6]^{4-}$ octahedra, the M-cations are located at the body centers, and six numbers of X-anions are placed at the face centers (*see* **Figures 2A,B**). The structure of perovskite materials mostly depends on the size of the A-site cation. The larger A-site cations do not fit inside the space and lead to the formation of lower-dimensional perovskite crystal structures. In the case of two-dimensional (2-D) perovskites (A_2MX_4), the longer cations are located at the A-site positions, and each $[MX_6]^{4-}$-octahedron is connected with four neighboring halide anions, which create a 2-D layered network structure as shown in **Figure 2C**. In the case of one-dimensional (1-D) perovskites ($A'AMX_5$), each octahedron is attached with two opposite corners, which form a series of parallel infinite chains (*see* **Figure 2D**). In the case of zero-dimensional (0-D) perovskites (A_4MX_6), each octahedron is separated by four A-site cations, which behave like an isolated molecule (*see* **Figure 2E**).

Defect Tolerance and Energy Diagram

Goldschmidt's tolerance factor is defined as $t = \frac{(r_A + r_X)}{\sqrt{2}\,(r_M + r_X)}$, where r_A, r_M, and r_X are the radius of respective ions in the AMX_3 formula, which hints at the formation of respective well-defined perovskite structures (Veldhuis et al., 2016; Kovalenko et al., 2017; Li et al., 2017; Akkerman et al., 2018; Yan et al., 2019; Li et al., 2020). For instance, the majority of the 3-D lead iodide

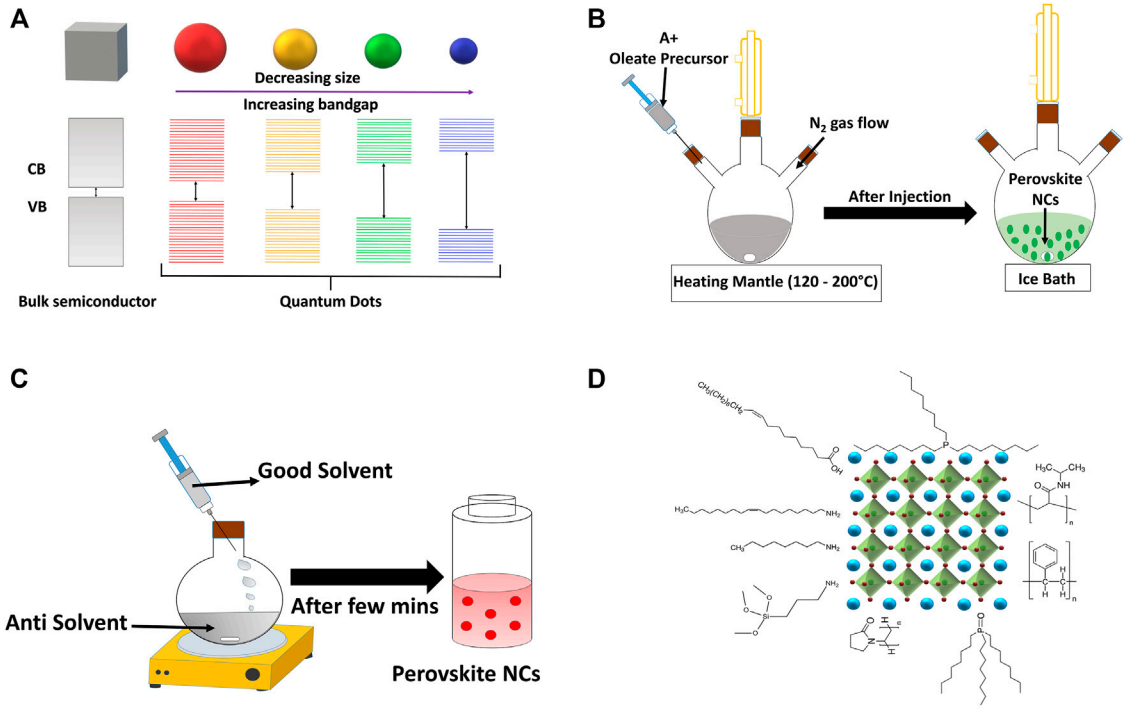

FIGURE 4 | (A) Quantum confinement effect in size tunable NCs, schematic representation of colloidal synthesis processes of perovskite NCs by **(B)** hot injection, **(C)** LARP, and **(D)** schematic diagram showing attachment of different ligands to a perovskite NC surface.

perovskite materials have t values ranging between $0.8 \leq t \leq 1.0$, which confirms the ideal cubic structure and possesses the most stable phase (*see* **Figure 3A**). If the t value is not in this range, then the crystal structure transforms into different crystal phases or forms lower-dimensional perovskites. The perovskite material, which has a t value that lies at the edge of the range 0.8–1.0, such as $FAPbI_3$ (t~ 1) and $CsPbI_3$ (t~ 0.8), can easily undergo a phase transition. Hence, the $FAPbI_3$ and $CsPbI_3$ cubic crystal structures transform to comparatively stable hexagonal and orthorhombic phases, respectively, at room temperature, which is referred to as yellow phases (*see* **Figures 3B,C**). The crystal stability of the perovskites can be enhanced by adjusting the t value close to 0.9. The perovskite structure is also restrained by the octahedral factor (μ), which is defined as $\mu = \frac{r_M}{r_X}$. It describes the stability of the $[MX_6]^{4-}$-octahedra which ranges from 0.442 to 0.895.

The energy level diagram of lead halide perovskites is dependent on the M-site and X-site ions. From a theoretical point of view, the energy of the emitted photon from perovskite materials can be relatable to the energy difference between the conduction band minimum and the valence band maximum. The valence band for lead halide perovskites is formed by the np orbitals of the X ions and the 6s orbitals of the Pb ions, whereas the conduction band is mainly determined by the Pb-6p orbitals with a minor contribution from the np orbitals of the X ions as shown in **Figure 3D** (Sum and Mathews, 2014). Henceforth, the absence of bonding–antibonding interaction between these conduction bands and valence bands (VB) results in a high defect tolerance. Thus, the maximum number of defect states lies within the valance or conduction bands instead of in between the bandgap. It has been observed an abrupt change in the bandgap energy with halide substitution in $MAPbX_3$ perovskites, which are 2.97, 2.24, and 1.53 eV for $MAPbCl_3$, $MAPbBr_3$, and $MAPbI_3$, respectively, with slight change in the ionic radii of Cl ions (1.81 Å), Br ions (1.96 Å), and I ions (2.20 Å) (Sum and Mathews, 2014; Correa-Baena et al., 2017). On the other hand, the bandgap energy of the $APbI_3$ perovskites changes very slightly with an exchange in A-site cations [$MAPbI_3$ (1.55 eV) > $CsPbI_3$ (1.5 eV) > $FAPbI_3$ (1.45 eV)], even though the ionic radii of the A-site cation change immensely in the range of 1.8–2.5 Å (Sum and Mathews, 2014; Correa-Baena et al., 2017).

INTRODUCTION TO NCS

NCs consist of about hundreds to thousands of atoms on the scale of 1–100 nm whose properties are similar to neither the individual atom nor those of the bulk materials (Roduner, 2006; Burda et al., 2005). If the size of NCs is less than the exciton Bohr radius then the energy levels of NCs split to each other due to the quantum size confinement effect and such NCs are defined as quantum dots (QDs). The charge carriers are spatially confined inside the QDs. The photophysical qualities immensely rely on size and shape of the QDs as shown in **Figure 4A**. A bulk solid contains very few numbers of surface atoms; as a result, broken chemical bonds have a minimal effect on the material properties. However, the smaller the NCs become,

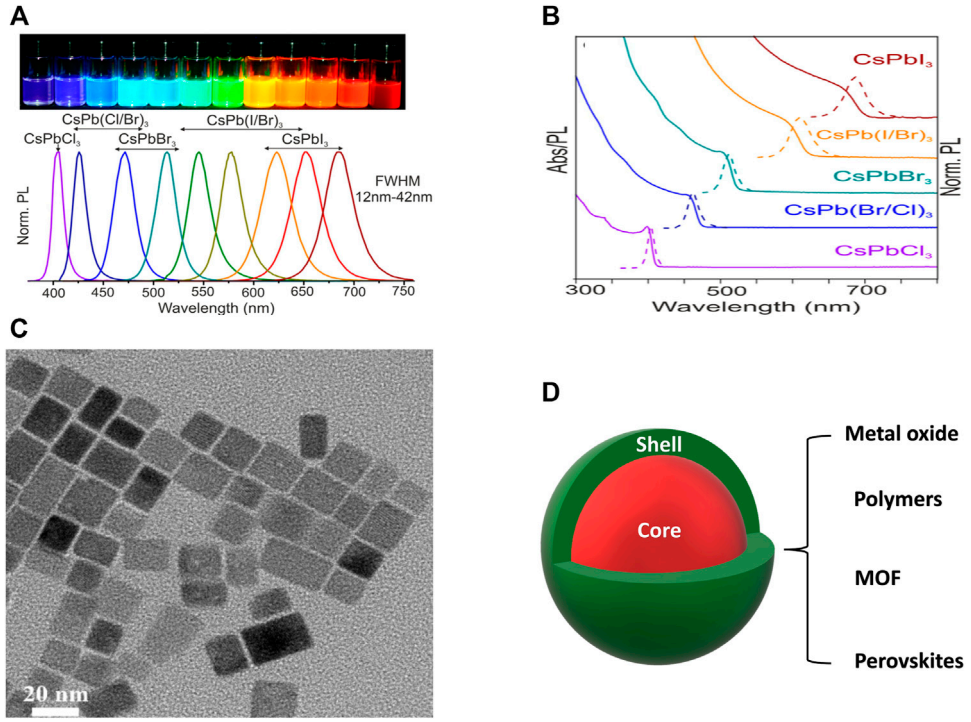

FIGURE 5 | (A) PL spectra of different halide perovskite NCs (Inset: photograph of the corresponding NCs in solution form under a UV lamp). **(B)** Absorption, PL spectra, and **(C)** TEM image of all inorganic $CsPbX_3$ perovskite NCs. **(D)** Schematic diagram of a core@shell NC structure. **(A,B)** are reproduced with permission from Protesescu et al. (2015). Copyright 2015, American Chemical Society. **(C)** is reproduced with permission from Chen et al. (2021a). Copyright 2021, Elsevier B.V. 3.1.2.

the more number of surface atoms combinedly affects the optical qualities of the NCs (Boles et al., 2016; Kazes et al., 2021). Size-dependent emission tunability, high intensity of emission, and narrow emission spectrum allow them to explore considerably in the fields of LEDs, solar cells, lasing, photodetectors, etc. (Shirasaki et al., 2013; Kramer and Sargent, 2014; García de Arquer et al., 2017; Liu et al., 2021).

Synthesis of Metal Halide Perovskite NCs

Various efforts have been made to develop dependable synthetic strategies for the preparation of high-yielding metal halide perovskite NCs by controlling their shape, restricting their size to nano-range and their optical properties (Kovalenko et al., 2017; Li et al., 2017; Akkerman et al., 2018; Yan et al., 2019; Li et al., 2020). These approaches can be classified either as top-down or as bottom-up methods. The top-down approach defines the fragmentation and structuring of macroscopic solids through a mechanical or chemical approach. At the same time, the bottom-up approach starts with molecules and ions, which proceed *via* liquid or vapor phase chemical reactions. It is observed that the liquid phase chemical reaction is the best way for synthesizing metal halide perovskite NCs. The two most developed liquid phase synthesis methods of colloidal metal halide perovskite NCs are hot-injection and ligand-assisted reprecipitation (LARP) methods. The hot-injection method requires an inert atmosphere and a high working temperature which makes NC synthesis costly and hence limits its mass production. However, the perovskite NCs can also be synthesized at room temperature *via* the LARP method that can be employed as the most cost-effective way to grow high-quality perovskite NCs.

Hot Injection Synthesis Strategy

Hot injection synthesis is a strategy where generally the precursor solution is rapidly injected into a hot solution. The hot solution consists of a high boiling solvent containing MX_2 halide precursors and ligands (*see* **Figure 4B**). (Li et al., 2017; Kovalenko et al., 2017; Akkerman et al., 2018; Yan et al., 2019; Li et al., 2020) This method is generally used for synthesizing NCs that exhibit a narrow size distribution, separating the nucleation and growth stages. Immediately after the injection, a rapid nucleation bursts resulting in the formation of small nuclei. Furthermore, due to the rapid depletion of monomers, the nucleation stage terminates and the nuclei starts growing over time and eventually forming NCs with narrow size distribution. The first report on metal halide perovskite synthesis *via* the hot-injection method was reported in 2015 by Protesescu et al. for the colloidal synthesis of $CsPbX_3$ NCs (Protesescu et al., 2015). The NCs were synthesized by injecting the Cs-oleate precursor into a hot solution of PbX_2 (X = Cl, Br, I) salts at 140–200°C, which were dissolved in octadecene (ODE) along with carboxylic acids and primary amines. The absorption and PL spectra of the resulting NCs are given in **Figures 5A,B**. The NCs are cubic in shape as shown in **Figure 5C**. It was observed that monodisperse NCs depend on equal ratios of acids and amines and the size can be

adjusted by simply changing the reaction temperature. Mixed-halide perovskite NCs can also be easily synthesized by merely changing chemical proportions of the halide salts (Akkerman et al., 2015; Nedelcu et al., 2015). PL emission of the resulting NCs could be finely adjusted across the entire visible spectrum (410–700 nm) by varying the halide composition and tuning the size of the NCs. Consequently, the hot-injection method was extended to $FAPbX_3$ (X = Br, I) NC systems by replacing Cs-oleate with formamidinium-oleate (Protesescu et al., 2016). In view of this, with passing years, different organic and inorganic metal halide perovskites have been synthesized by this method with control over size and shape of resulting NCs by varying the reaction time, ligands, temperature, and precursor concentrations (Pan et al., 2016; Sun et al., 2016).

LARP Synthesis Method

LARP is merely a simple process compared with the hot-injection method, which consists of dissolving the respective ions in a good solvent up to a certain equilibrium concentration and then transferring the solution into a state of nonequilibrium, i.e., supersaturation (*see* **Figure 4C**) (Kovalenko et al., 2017; Li et al., 2017; Akkerman et al., 2018; Yan et al., 2019; Li et al., 2020). The supersaturated state can be raised by varying the temperature, i.e., cooling down the solution, by evaporating the solvent, or by adding a miscible cosolvent in which the solubility of the ions is low. Under these conditions, spontaneous precipitation and re-crystallization reactions occur until the system reaches an equilibrium state. If this procedure is implemented along with ligands, then this process is referred to as LARP method. The desired organic or inorganic salts (MAX, CsX, or PbX_2) are dissolved in suitable polar solvents, i.e., dimethylformamide (DMF) or dimethylsulfoxide (DMSO), and then the precursor solution is injected in poor solvents such as toluene, hexane, or octane, along with suitable ligands or any other capping reagents. When the precursor solution is injected into the poor solvent, the mixture results in a supersaturation instantly, inducing the growth and nucleation of perovskite NCs. It is to be noted that the LARP procedure can be implemented under normal atmospheric conditions by using simple chemical equipment and can be easily multiplied, which allows production of metal halide perovskite NCs on a large scale. Also, these NCs are well distributed and possess a narrow size distribution. The first report on the LARP synthesis of organic–inorganic $MAPbBr_3$ NCs was presented by Schmidt et al.; the perovskite precursor salts were mixed in DMF and injected dropwise in toluene. It formed moderately luminescent green NCs with sizes 6 nm (Schmidt et al., 2014). Later, various color-tunable and highly luminescent perovskite NCs were synthesized *via* the LARP method (Kovalenko et al., 2017; Li et al., 2017; Akkerman et al., 2018; Yan et al., 2019; Li et al., 2020).

Stability Issues in Metal Halide Perovskites

The instability of metal halide perovskites remains a major issue that needs to be tackled soon because the perovskite structures readily undergo chemical degradation, resulting in optical losses (Park and Seok, 2019; Zhao and Park, 2015; Zhou and Zhao, 2019). They degrade very easily due to their ionic nature. These perovskite crystals suffer from chemical instability against moisture, oxygen, and polar solvents. The attachment of ligands on the surface of NCs is not very strong. They can detach effortlessly, which results in agglomeration of NCs *via* an oriented attachment process (Baranov et al., 2021; Bhaumik, 2019). This leads to transformation into larger crystals and losses of NC properties in the nanometer regime. Also, mixing different compositions of perovskite NCs leads to an anion-exchange process, resulting in the shifting in the PL emission, deteriorating their initial optical stability. Recently, various research progress has been achieved to improve the NC stability through compositional engineering, development of the 2-D structures interlinked by long-chain organic molecules (*see* **Figure 4D**) (Kamat et al., 2020; Ahmed et al., 2021; Kar et al., 2021). An encapsulating shell over the perovskite NCs is a suitable approach to improve the stability from the harsh external atmosphere and enrich the core's optical properties.

Encapsulation of Perovskite NCs With Different Shelling Materials

The term encapsulation is usually referring to coating of a protective layer around the NCs during or after the synthesis. The aim is to achieve homogenous dispersion of emitting NCs into a single or a matrix of protective shell to reduce agglomeration and quenching of PL. Many approaches have been made by coating the perovskite NC core with some acceptable coating materials such as various metal oxides, metal-halide perovskite, metal organic framework, polymer (*see* **Figure 5D**).

Zheng and his coworkers synthesized silica-encapsulated $MAPbBr_3$. They prepared $PbBr_2$, MABr, and APTES precursors mixed in DMF which were injected into toluene. Silica-coated $MAPbBr_3$ NCs were synthesized, followed by the hydrolysis and condensation of tetraethyl orthosilicate (TEOS), forming a silica coating. The PL peak with quantum yield 60.3% was obtained at 523 nm (Zeng et al., 2018). Yang and his coworkers reported an approach in which they used aminopropyl trimethoxy silane (APTMS) in place of aminopropyl triethoxy silane (APTES) to form orthorhombic $MAPbBr_3@SiO_2$ (Yang et al., 2018). The orthorhombic phase of NCs was stable after silica encapsulation and was highly luminescent. The PL emission peak was obtained at 527 nm and a QY of 78%. The shape of the NCs was spherical with an average diameter of 2.8 nm. Other than silica, titanium oxide (TiO_2) has also been used as an oxide material to encapsulate on the surface of $CsPbBr_3$ NCs (Li et al., 2018). According to the analysis they observed a decrease in PL intensity due to the type-II band alignment of these core@shell NCs than that of normal $CsPbBr_3$ NCs. $CsPbBr_3@TiO_2$ NCs had an orthorhombic phase and exhibited PL peak at 520 nm. The NCs were stable for 12 weeks in aqueous media, demonstrating high water stability of these core@shell NCs.

Bhaumik and his coworkers reported a unique approach for synthesizing $MAPbBr_3$ core and octylammonium lead bromide $(OA)_2PbBr_4$ shell NCs (Bhaumik et al., 2016). The molar ratios of

MABr and OABr were varied to obtain different thicknesses of shell layer around the core. The pure $MAPbBr_3$ NCs showed an absorption peak at 513 nm and a PL peak at 521 nm with a QY of 84%. With an increase in the concentration of OABr, additional peaks were seen at lower wavelength in the absorption spectra. The PL emission peaks were also shifted toward the lower wavelength side, confirming the presence of a layered perovskite structure over the surface of core. The 8:2 M ratio of MABr and OABr gave the best QY of 92% with impressive stability for above 2 months under a normal atmospheric condition. The average size of NCs observed from the TEM images was in the range of 5–12 nm. Novel $CsPbBr_3$@$CsPbBr_x$ core@shell NCs were synthesized *via* the hot-injection method (Wang et al., 2018b). The size of NCs was obtained as 6 nm, while the size of core was 2 nm. The NCs showed an emission peak at 463 nm with QY of 84%, which was much higher than the pure $CsPbBr_3$ NCs (QY~ 54%). The protective amorphous $CsPbBr_x$ shell helps the excited charge carriers to accumulate inside the core and improve the NC luminescence intensity. This shell also protects from direct contact with harmful atmospheric oxygen and water molecules that degrade the perovskite structure. Another report of $CsPbX_3$@Cs_4PbX_6 core@shell NCs was synthesized *via* the hot-injection method (Jia et al., 2018). The core NCs were cubic in shape with an edge width of 7.2 nm. However, with Cs_4PbBr_6 shelling, the width of the core@shell NCs increased. The PL peak was obtained at 516 nm with a QY of 96.2% compared with the QY 84.4% of core NCs.

Besides metal oxides and perovskite shells, MOFs are another suitable shelling material for perovskite NCs forming composites since they have a very high surface area. Kong and his coworkers synthesized $CsPbBr_3$@Zerolite imidazole framework photocatalyst, which then showed enhanced CO_2 reduction compared with normal $CsPbBr_3$ (Kong et al., 2018).

Coating NCs with suitable polymers is another way of increasing material stability. For the effective passivation of the NC surface, the preferred polymer can be introduced at the synthesis stage or post synthesis eventually forming a polymer shell or a matrix around the NCs. The selectivity of the polymer is generally based on the final material's specific advantages, which leads to flexibility, hydrophobicity, or biocompatibility. Raja et al. reported that the poly(styrene-ethylene-butylene-styrene) (SEBS) was mixed with NCs ($CsPbBr_3$), which significantly improved the water stability for nearly 4 months (Raja et al., 2016). Also, the samples showed more than 200 times less Pb atoms than the one that contained unprotected NCs. They also studied the interaction of poly(lauryl methacrylate) (PLMA) with these NCs. The composites were highly stable in an ambient environment and partially soluble in an aqueous medium. Huang and his coworkers reported $CsPb(Cl/Br)_3$ NCs dispersed with ethyl-cellulose, spin-coated onto optical glass (Huang et al., 2019). The stability of the NCs was more than 5 days under environmental conditions. Wang and his coworkers coated $MAPbBr_3$ NCs with various polymers such as polymethyl methacrylate (PMMA), polyvinyl chloride (PVC), cellulose acetate, acetonitrile butadiene styrene (ABS), polycarbonate (PC), and polystyrene (PS) and studied their optical properties under different conditions (Wang et al., 2016). The polymer-coated film was prepared by the swelling and de-swelling technique, which enables polymer dissolution in suitable solvents. During the evaporation process, shrinkage in polymers occurs, forming a strong binding on the NC layer. Then the water stability of the films in the above-discussed polymer matrices was performed. A slight decrease in QY was observed after boiling the polycarbonate and polystyrene-coated films for 30 min. In addition, polycarbonate films can withstand up to 180°C exhibiting a high thermal stability. Zhang et al. synthesized NCs in micro-hemispheres of polystyrene matrix (Zhang et al., 2017). The polymer PVP was added to perovskite precursors to passivate the surface and further the PVP-passivated NC solution was injected into the PS solution. Owing to the interfacial tension, PS molecules aggregate into spherical micelles with NCs trapped inside them. The spherical micelles form micro-hemispheres when the resulting solution is dropped onto a quartz substrate under the effect of gravity.

KEY PARAMETERS OF WLEDS

The major parameters for the characterization of LED to be considered when developing luminescent materials for WLEDs are CCT, CRI, LE, and CIE 1931 (x,y) color space.

CCT is meant to identify the color temperature of any light source (Wood and Bulović, 2010). Ideally, a pure white light source should have a CCT value between 2500 and 6500 K. Light sources with CCT values above 5000 K represent bluish-white light sources, whereas temperatures below 4000 K signify yellowish light sources (i.e., incandescent lamps). However, it is difficult to represent a complex spectral distribution of a light source with a simple CCT number. Therefore, many other parameters are used to define the quality of any light source. CRI is represented as a quantitative measure of a light source to reveal the colors in comparison with natural or standard light sources (Wood and Bulović, 2010). It is measured on a scale of 0–100, where 100 is known as the illumination of a standard light source where daylight and incandescent bulbs are used as typical reference sources. When the CRI value is low, the colors are somewhat saturated (with pale aspect) or too saturated (with vivid appearance). The CRI value for white light is considered to be 80 (Nardelli et al., 2017).

The CIE maps the color of a light source in terms of hue and saturation (Wood and Bulović, 2010). The boundary of the CIE color diagram can be identified by the different saturated hues perceived by the human eye in wavelength range from 380 to 780 nm. The color purity defines the closeness to the boundary of the CIE diagram. The color gamut can be enabled by a display with a triangle where red, green, and blue (RGB) pixels define the color coordinates of the individual pixels. The triangle of RGB-NCs is larger than the International Telecommunication Union HDTV standard, highlighting the advantage of NC emitters. The CIE color coordinates for WLED must have lied close to the value of (0.33, 0.33) (Wood and Bulović, 2010). LE is defined as a measurement of brightness based on a standardized model of the human eye's sensitivity, which can be measured by the ratio of luminous flux to input power (Lumens/Watt in SI unit). High LE

requires high light extraction from an LED package which should be in between 20 and 60 Lumens/Watt for an efficient WLED. The antisenility of phosphors and epoxy can directly influence the lifespan of WLEDs.

UTILIZATION OF METAL HALIDE PEROVSKITES IN WLED APPLICATIONS

Blue LED + Red/Yellow Phosphor + Metal Halide Perovskite NCs

In WLED applications based on red/yellow phosphor, the generation of white light generally has low color-rendering index as the spectrum has less green/red components, respectively. Henceforth, red and green halide perovskite NCs can improve the color-rendering index and reduce the color temperature values by placing them onto a phosphor-converted WLED.

In the context of this, Xu and his coworkers reported the synthesis of $CsPbBr_3$ NCs *via* the hot-injection method, where olive oil was used in the place of oleic acid as a surfactant (Xu et al., 2019). QY was achieved up to 93%. The WLED was fabricated by mixing the $CsPbBr_3$ NCs with K_2SiF_6:Mn^{4+} phosphors that were blended with silicone resin A and silicone resin B in the ratio of 1:1 and then sintering at 120°C for 30 min. Finally, the mixture was directly coated onto a blue LED chip (453 nm). Under an operating voltage of 3 V, the WLED exhibited a high CRI of 85, an LE of 46 Lumens/Watt, a CIE of (0.34, 0.31), a CCT of 4754 K, and a color gamut of 118% of NTSC standard. Xuan and his coworkers reported the synthesis of $CsPbBr_3$ nano-crystals synthesized *via* hot injection and then embedded into super-hydrophobic porous organic polymer frameworks ($CsPbBr_3$@SHFW) (Xuan et al., 2019). The composites exhibited a QY of 60% and showed better water stability due to super hydrophobicity. The respective WLED was fabricated by encapsulating a mixture of $CsPbBr_3$@SHFW composites, KSF phosphors, and silicone resin onto a blue InGaN LED (447 nm). It exhibited a high LE of 50 Lumens/Watt at a driving current of 20 mA. The corresponding EL spectrum consisted of three emissions peaks centered at 447 nm, 525 nm, and 630 nm. The WLED showed a CIE value of (0.329, 0.305) and a color gamut of 127% of NTSC standards.

Furthermore, Chen and his coworkers reported the synthesis of $CsPbX_3$ NCs by using peanut oil as a ligand source (Chen et al., 2019). QY of the NCs was obtained as high as 96.9%. First, the green-emitting $CsPbBr_3$ PNCs, red-emitting (Sr, Ca) $AlSiN_3$:Eu^{2+} phosphors, and epoxy resin were mixed. This mixture was then coated on a GaN blue LED chip to complete the fabrication of a WLED. The WLED exhibited a white light emission which showed a CIE value of (0.4050, 0.3985), a CRI value of 81.1, and a CCT value of 3529 K. Xu and his coworkers prepared $CsPbX_3$ NCs *via* a hot injection method. They studied the phase transition from monoclinic to cubic $CsPbX_3$ NCs, which helped to understand the growth and synthetic kinetics of these NCs better (Xu et al., 2020). The obtained QY was 99.8%. They fabricated a WLED by combining green-emitting NCs with red-emitting KSF phosphors with silicone resin. The anhydride curing agent in the ratio of (1:2) was coated onto a blue LED (453 nm) and then thermally cured at 120°C for 2 h. The WLED showed the CIE value of (0.389, 0.376) at a driving current of 20 mA with a wide color gamut of 123% compared with NTSC standards. Furthermore, Li et al. synthesized and encapsulated porous Y_2O_3 nanoparticles (P-Y_2O_3) on $CsPbBrI_2$ PNCs using a porous-nanoparticle-assisted dispersion strategy (Li et al., 2022). The corresponding WLED device was fabricated by combining the as-prepared $CsPbBrI_2$/Y_2O_3 composite and YAG: Ce^{3+} yellow phosphor on an InGaN blue chip (460 nm). The fabricated WLED provided white light emission at a driving current of 5 mA. Two discrete peaks were observed for composite-based LED in the blue and green-to-red regions. The EL spectra of the WLEDs are shown in **Figure 6A**. As a result, the CIE value of the fabricated WLED was (0.339, 0.354) with a CCT value of 5049 K (*see* **Figure 6C**). The LE of the as-prepared WLED was obtained at 61 Lumens/Watt with a CRI of 83. Besides the 3-D perovskites, Fang et al., in 2021, reported a 2-D layered perovskite with high quantum yields and enhanced stability. They synthesized Mn-doped $PEA_2(Pb/Mn)(Br/I)_4$ PNCs by anion exchange surface engineering. They achieved a QY of 52%, which was comparable to most of the reported red-emitting phosphors (Fang et al., 2021). They fabricated a WLED by using commercial (Sr, Ba)$_2SiO_4$:Eu phosphor and $PEA_2(Pb/Mn)(Br/I)_4$. The mixture was then dispersed in PMMA/toluene solution and coated onto a quartz glass. These color converters were finally incorporated onto a blue LED (440 nm) chip. The corresponding WLED had a white light emission (*see* **Figure 6B**) with a CIE value obtained at (0.34, 0.33).

Later, Shu et al. incorporated $CsPbX_3$ PNCs in an aluminum stearate ($AlSt_3$) matrix *via* the co-precipitation approach (Shu et al., 2021). $AlSt_3$ used as a hydrophobic shell to protect $CsPbBr_3$ PNCs from the environment. These shells passivate the PNC surface *via* the coordination bonding formed between St-Cs and St-Pb and bonding between the Al^{3+} and Br^-ions. They fabricated a WLED combining $CsPbBr_3$@$AlSt_3$ composites on a N620 phosphors. Epoxy was deposited on a blue-emitting InGaN chip. As a result, the device obtained bright white light with a CRI (R_a) of 90, a CCT (Tc) of 4929 K, and a CIE of (0.34, 0.32) (*see* **Figure 6E**). The crafted WLED possessed excellent R_a compared with commercially used WLEDs with low R_a (<80). Furthermore, there was no significant change in R_a and Tc after continuous operation of 24 h. Renjie Chen et al. synthesized $CsPbBr_3$ NCs and doped them with zinc ions to improve their optical properties and stability due to the enhancement in the formation of energy and surface passivation (Chen et al., 2021a). The doped NCs were synthesized *via* the hot-injection method achieving a QY of 91.3%. The respective WLED was fabricated by combining the Zn-doped $CsPbBr_3$ NCs and K_2SiF_6:Mn^{6+} phosphors onto a blue LED chip exhibiting LE of 36 Lumens/Watt (*see* **Figure 6D**) with a CIE value obtained at (0.327, 0.336), as shown in **Figure 6F**. A CCT value of 5760 K and a wide color gamut of 137% of the NTSC standard were obtained.

Li and his coworkers reported the room-temperature synthesis of silica-coated di-dodecyl dimethylammonium bromide (DDAB)-capped $CsPbBr_3$ NCs (Li et al., 2021b). The DDAB-coated $CsPbBr_3$ encapsulated by SiO_2 NC composites exhibited

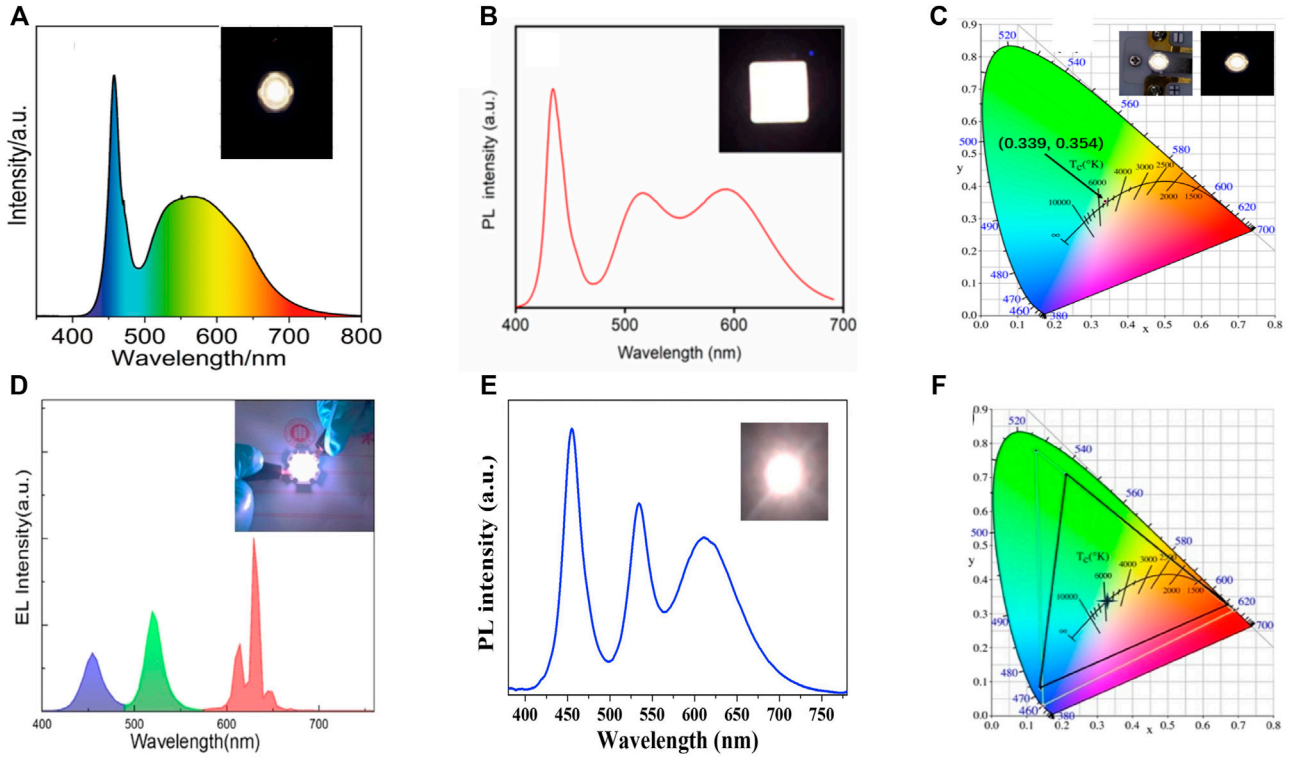

FIGURE 6 | (A) EL spectrum of $CsPbBrI_2/Y_2O_3$ composite-based WLED. **(B)** EL spectra of WLED based on $(Sr,Ba)_2SiO_4$:Eu phosphor and $PEA_2(Pb/Mn)(Br/I)_4$. (Inset of a and b is the photograph of WLED under the external bias.) **(C)** CIE coordinates of $CsPbBrI_2/Y_2O_3$ composite-based WLED. **(D)** EL spectrum based on Zn-doped $CsPbBr_3$ NCs, KSF phosphors, and a blue LED chip (the inset photograph shows the WLED under working condition). **(E)** EL spectra of WLED fabricated by depositing the mixture of $CsPbBr_3$-$AlSt_3$ composites and nitrate phosphors. **(F)** The color coordinate and the color gamut of as-fabricated WLED based on Zn-doped $CsPbBr_3$ NCs, KSF phosphors, and a blue LED chip. **(A,C)** are reproduced with permission from Li et al. (2022). Copyright 2021, Elsevier Ltd. **(B)** It is reproduced with permission from Fang et al. (2021). Copyright 2021, Elsevier B.V. **(D,F)** These are reproduced with permission from Chen et al. (2021a). Copyright 2021, Elsevier B.V. **(E)** It is reproduced with permission from Shu et al. (2021). Copyright 2021, Elsevier B.V.

an improved QY and a higher stability in ethanol and heat than that of pure $CsPbBr_3$ and DDAB-capped $CsPbBr_3$ (*see* **Figure 7A**). As a result, the WLED was fabricated by depositing green DDAB-capped $CsPbBr_3$ encapsulated by SiO_2 NC composites and red InAgZnS NCs as a color-conversion layer on a blue LED for warm white WLEDs. **Figures 8A–C** show the PL spectra of WLEDs based on DDAB-capped $CsPbBr_3$, DDAB-capped $CsPbBr_3$ encapsulated by SiO_2 NCs, and pure $CsPbBr_3$ at a voltage of 2.6 V, respectively. The PL intensities of DDAB-capped $CsPbBr_3$ and DDAB-capped $CsPbBr_3$ encapsulated by SiO_2 were more than the pure $CsPbBr_3$, for which there was a shift in color coordinates toward green, resulting in a better CRI of 86, a CIE value of (0. 41, 0.38) of DDAB-$CsPbBr_3/SiO_2$ composites. The CCT value of 3209 K and a high-power efficiency of 63.4 Lumens/Watt at a driving voltage of 3 V for DDAB-$CsPbBr_3/SiO_2$ composites, while those based on DDAB-$CsPbBr_3$ showed a low CRI of 73.

Yan et al. reported ligand-modified $CsPbBr_3$ NCs where they used 2-hexyldecanoic acid (DA) so as to replace the normal oleic acid (OA) (Li et al., 2021a; Dongdong et al., 2022). Furthermore, two WLEDs were constructed by combining the ligand-modified $CsPbBr_3$ NCs (OA/DA) with AgInZnS NCs on InGaN blue chip. The EL spectra of OA-capped $CsPbBr_3$, and DA-capped $CsPbBr_3$ are shown in **Figures 8D,E** (the inset images show the cold white and warm white LED of OA and DA-capped $CsPbBr_3$). The DA-capped $CsPbBr_3$ showed the CIE of (0.44, 0.42), a high CRI of 93, and an LE of 64.8 Lumens/Watt. A comparative study of both CRI and CCT values of all the composites from **Figures 8A–E** is shown in **Figure 8F**. This comparative study provides a clear understanding between DDAB-capped $CsPbBr_3$ and OA/DA-capped $CsPbBr_3$-fabricated white LED from pure $CsPbBr_3$. It is being noticed that a high CRI value (93) and a lower CCT value (3018 K) were obtained for DA-capped $CsPbBr_3$. Later, Shen et al. reported a WLED based on a cyan-emitting (trimethylsilyl) methylamine (TmMA)-modified $(MA)_x(DMA)PbBr_{3+x}$ lower-dimensional perovskite with cyan emission (Shen et al., 2021). They achieved a QY up to ~87.8%. The WLEDs were fabricated with the commercial YAG: Ce phosphor, $CaAlSiN_3:Eu^{2+}$ red phosphors, and cyan-emitting perovskite applied onto a blue LED InGaN chip. The WLED exhibited white light emission with a CIE value at (0.31, 0.34) with a CCT value of 6677 K. The CRI value was 81.7 of TmMA-modified cyan-emitting perovskite nano-crystals, much higher than the conventional WLEDs, i.e., without the TmMA-modified perovskite material (CRI~ 73.1) as shown in **Figure 7B**. The WLED also exhibited an internal quantum efficiency (IQE) of nearly 68.5%.

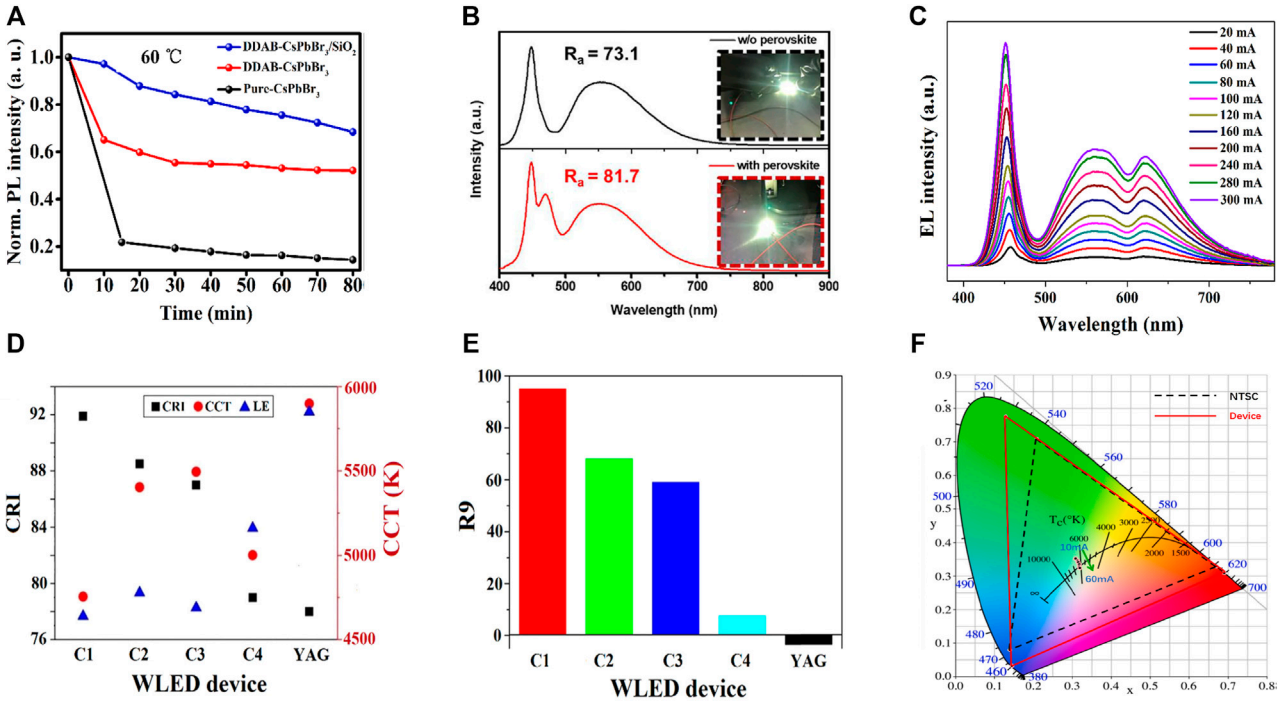

FIGURE 7 | (A) PL intensities of pure $CsPbBr_3$ QD, DDAB-$CsPbBr_3$ QD, and DDAB-$CsPbBr_3/SiO_2$ QD composites under a continuous heating at 60°C as a function of heating time. **(B)** Emission spectra of WLEDs based on PEABr and TmMA-modified $(MA)_x(DMA)PbBr_{3+x}$. (Inset: photographs of corresponding working WLEDs). **(C)** CRI, CCT, and LE of WLEDs C1 to C4 and YAG:Ce. **(D)** EL spectra of C1-based WLED operated at working currents of 20–300 mA. **(E)** R9 of WLEDs C1 to C4 and YAG:Ce. **(F)** Color gamut of the white LED based on PQD solid powders and red $K_2SiF_6:Mn^{4+}$ phosphor with a blue LED. **(A)** It is reproduced with permission from Li X. et al. (2021). Copyright 2021, Elsevier B.V. **(B)** It is reproduced with permission from Shen et al. (2021). Copyright 2021, Elsevier B.V. **(C–E)** These are reproduced with permission from Tang et al. (2022). Copyright 2021, Elsevier B.V. **(F)** It is reproduced with permission from Chen et al. (2021b). Copyright 2021, Elsevier Ltd.

In addition to the previous reports, Zhao et al. synthesized $MAPbBr_3$ PNCs and encapsulated them with hexagonal boron nitride (*h*-BN) to form *h*-BN/$MAPbBr_3$ PNC nanocomposites by the LARP approach (Zhao et al., 2022). Due to the excellent thermal conductivity and the layered structure of the *h*-BN material, the nanocomposite powder exhibits excellent thermal and moisture stability with a QY of 93.7%. As a result, the fabricated WLEDs with *h*-BN/$MAPbBr_3$ PNC nanocomposite, a commercial red phosphor, and a blue phosphor possessed CIE value of (0.35, 0.34), a CCT value of 4742 K, and 63.1 Lumens/Watt LE at a driving current of 20 mA. The color gamut of the fabricated WLED was 99.8% of the NTSC standard. The CRI value was found to be 75.

Tang et al. proposed a one-pot anchoring process in which they synthesized $MAPbBr_{0.5}I_{2.5}$ NCs and formed a composite with YAG:Ce (Tang et al., 2022). They have prepared four kinds of $MAPbBr_{0.5}I_{2.5}$ PNC@A-YAG composite by changing the amount of A-YAG and without A-YAG named C1, C2, C3, and C4, respectively. A WLED was fabricated by combining InGaN chip and A-YAG combined NC composite. **Figure 7C** represents the EL intensities of both YAG and PNCs increased with current from 20 to 300 mA, indicating that C1 composite exhibited no saturation. The CRI of 92, CCT of 4755 K, and a high R9 of 95 at an operational current of 20 mA were obtained (*see* **Figure 7D**). The CIE coordinates for the WLED were obtained at (0.34, 0.32), and an LE was obtained at 23.5 Lumens/Watt. They also performed the color stability against increasing current and concluded no saturation to the blue light within a wide range of working currents. All the optical properties, including CRI, CCT, and LE of the fabricated WLEDs, were observed. From YAG composite to C1–C4 composites, the CRI value was higher, and CCT was lower. But there was a decrease in LE for enhanced red emission. They also noticed that the R9 value corresponds to the CRI of saturated red, which had vital importance in producing warm white light. It was greatly enhanced from −3.5 for YAG to 95 for C1 composite (*see* **Figure 7E**).

In 2022, Qi et al. reported a unique approach for synthesizing $CsPbI_3$ PNCs in the borosilicate glass by melting-quenching and heat treatment (Qi et al., 2022). The corresponding WLED was fabricated by combining red $CsPbI_3$ PNC@glass and green commercial phosphor (LuAG: Ce) onto a blue LED chip. They adjusted the ratio of LuAG and red $CsPbI_3$ PNC@glass powder to contribute to bright white-light luminescence. The WLED yielded a CRI of 95, a CCT of 5755 K, and an LE of 95 Lumens/Watt under a driving current of 20 mA. With respect to the previous ones, the silica coating upon the NCs was reported by Zhihao

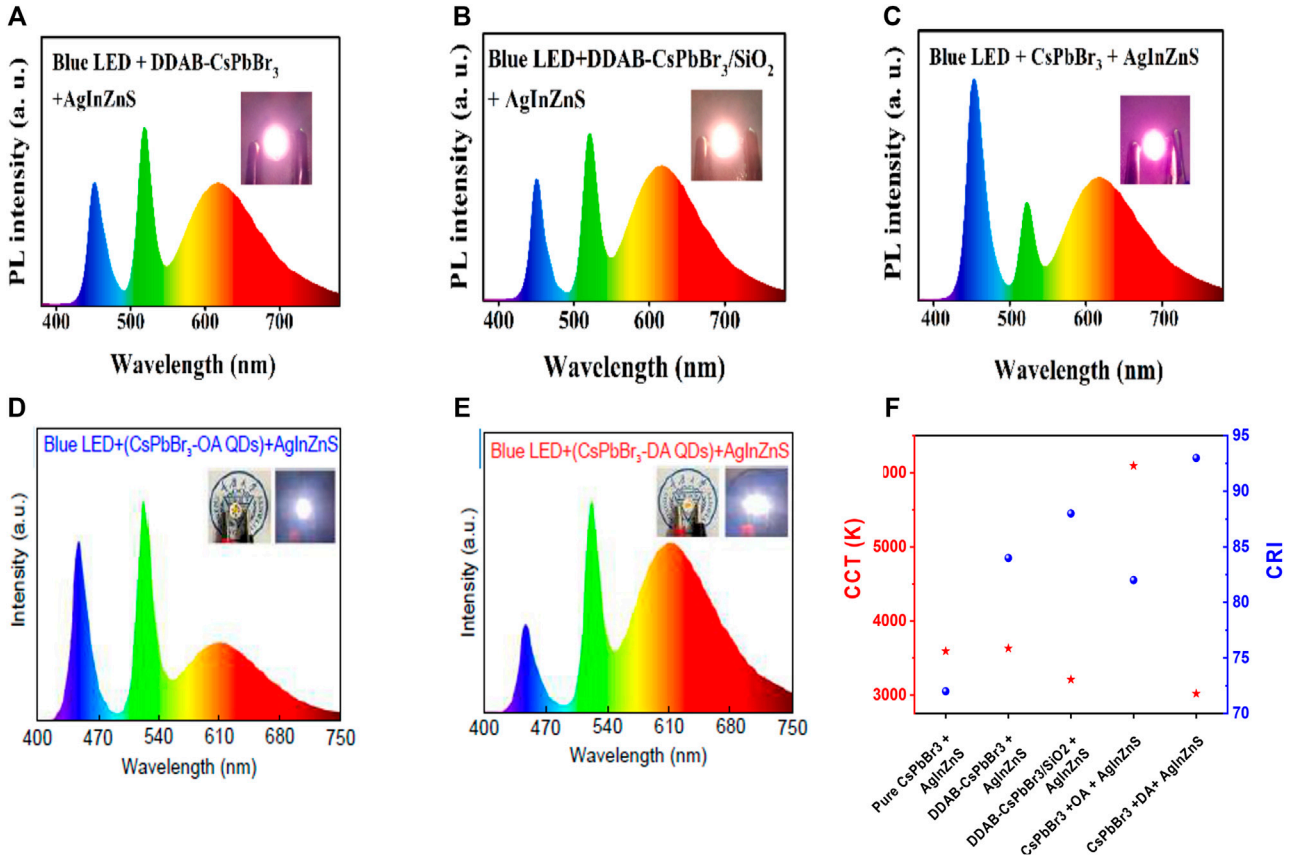

FIGURE 8 | EL spectra of WLEDs based on combination of **(A)** DDAB-$CsPbBr_3$ and AgInZnS QDs, **(B)** DDAB-$CsPbBr_3/SiO_2$ and AgInZnS QDs, and **(C)** pure $CsPbBr_3$ and AgInZnS QDs. (The inset of a, b, c show photographs of working WLEDs at a driving voltage of 2.6 V.) EL spectrum of WLEDs based on **(D)** $CsPbBr_3$-OA and AgInZnS QDs, and **(E)** $CsPbBr_3$-DA and AgInZnS QDs. (Inset shows photographs of the devices without and with driving voltage.) **(F)** Comparative CCT and CRI of all above-mentioned materials. **(A–C)** are reproduced with permission from Li X. et al. (2021). Copyright 2021, Elsevier B.V. **(D,E)** are reproduced with permission from Dongdong et al. (2022). Copyright 2022, OEA.

Chen et al. They synthesized $CsPbX_3$ by APTMS as ligands at room temperature (Chen et al., 2021b). The $CsPbBr_3$ was synthesized by the hot-injection method with a QY of 69.2%. They fabricated a white LED by combining the green $CsPbBr_3$ NCs and commercial red K_2SiF_6:Mn^{4+} phosphor with a blue LED chip (455 nm). The fabricated WLED emitted white light with CIE coordinates obtained at (0.3142, 0.3448) operated at 60 mA as shown in **Figure 7F** and an LE of 70.47 Lumens/Watt. Moreover, the color gamut of this WLED covered over 129.4% of the NTSC standard, suggesting that the prepared PNC solid powders possess great potential for the wide color gamut display application.

Similarly, Zhang et al. synthesized $CsPbBr_3$ NCs by introducing a double-terminal ligand 4,4′-azobis(4-cyanovalericacid) (CA) replacing oleic acid (OA) ligand at room temperature. They achieved a QY of 72% (Zhang et al., 2021). The white LED device was fabricated by using green-emitting $CsPbBr_3$-CA, commercial red-emitting K_2SiF_6:Mn^{4+} mixed with silicone resin B and silicone resin A with the ratio of 1:1 onto a blue LED chip (460 nm) and sintered for 2 h at 120°C in an oven. The device exhibited warm white light emission with CIE coordinates obtained at (0.33, 0.33) with an LE of 18.9 Lumens/Watt and a CCT value of 5569 K under a driving current of 20 mA and 2.6 V. A wide color gamut of more than 126% of NTSC standard was obtained from the WLED. In the meantime, Du et al. synthesized $CsPbBr_3/CsPb_2Br_5$@PbBr(OH) nano/microspheres through a water-assisted process by varying water content (Du et al., 2021). These microspheres had ultrahigh stability, and by mixing green-emitting PNC@PbBr(OH) powder and K_2SiF_6:Mn^{4+} (KSF) red phosphor on a 460-nm blue chip, a WLED were fabricated, which had a high luminous efficacy of 101.27 Lumens/Watt at 10 mA and CIE value obtained at (0.32, 0.33). The summary of the fabricated WLEDs by using perovskite NCs with blue chip and red/green phosphors is shown in **Table 1**.

Blue LED Chip + Metal Halide Perovskite NCs

Apart from integrating red or green perovskite NCs into YAG: Ce^{3+} based yellow phosphor and KSF phosphor-converted

TABLE 1 | Chart for different parameters of WLEDs fabricated by embedding perovskite NCs and phosphors upon a blue LED chip.

S.I No	Perovskite material	Synthesis method	CIE color coordinates	CCT (K)	CRI	LE (Lumens/Watt)	Color gamut (compared to NTSC)	References
1	Olive oil-capped $CsPbBr_3$	Hot-injection	0.34, 0.31	4754	85	46	118%	Xu et al. (2019)
2	$CsPbBr_3$@SHFW	Hot-injection	0.329, 0.305	—	—	50	127%	Xuan et al. (2019)
3	Peanut oil-capped $CsPbBr_3$	LARP	0.4050, 0.3985	3529	81.1	—	—	Chen et al. (2019)
4	$CsPbBr_3$	Hot-injection	0.389, 0.376	—	—	—	123%	Xu et al. (2020)
5	$CsPbBrI_2$@P-Y_2O_3	LARP	0.34, 0.35	5049	83	61	—	Li et al. (2022)
6	$PEA_2(Pb/Mn)$ $(Br/I)_4$	Hot-injection	0.34, 0.33	—	—	—	—	Fang et al. (2021)
7	$CsPbBr_3$@$AlSt_3$	LARP	0.34, 0.32	4929	90	—	—	Shu et al. (2021)
8	Zn-doped $CsPbBr_3$	Hot-injection	0.327, 0.336	5760	—	36	137%	Chen et al. (2021a)
9	DDAB-$CsPbBr_3/SiO_2$	LARP	0.41, 0.38	3209	88	63.4	—	Li X. et al. (2021)
10	DA-capped $CsPbBr_3$	Hot-injection	0.44, 0.42	3018	93	64.8	—	Dongdong et al. (2022)
11	$(MA)_x(DMA)PbBr_{3+x}$@TmMA	LARP	0.31, 0.34	6677	81.7	—	—	Shen et al. (2021)
12	*h*-BN/$MAPbBr_3$	LARP	0.35, 0.34	4742	75	63.1	99.8%	Zhao et al. (2022)
13	$MAPbBr_{0.5}I_{2.5}$@A-YAG	One-pot anchoring	0.34, 0.32	4755	92	23.5	—	Tang et al. (2022)
14	$CsPbI_3$@ borosilicate glass	Melt-quenching	—	5755	95	95	—	Qi et al. (2022)
15	$CsPbBr_3$@SiO_2	Hot-injection	0.3142, 0.3448	—	—	70	129.4%	Chen et al. (2021b)
16	CA-capped $CsPbBr_3$	LARP	0.33, 0.33	5569	—	18.9	126%	Zhang et al. (2021)
17	$CsPbBr_3/CsPb_2Br_5$@PbBr (OH)	LARP	0.32, 0.33	—	—	101.27	—	Du et al. (2021)

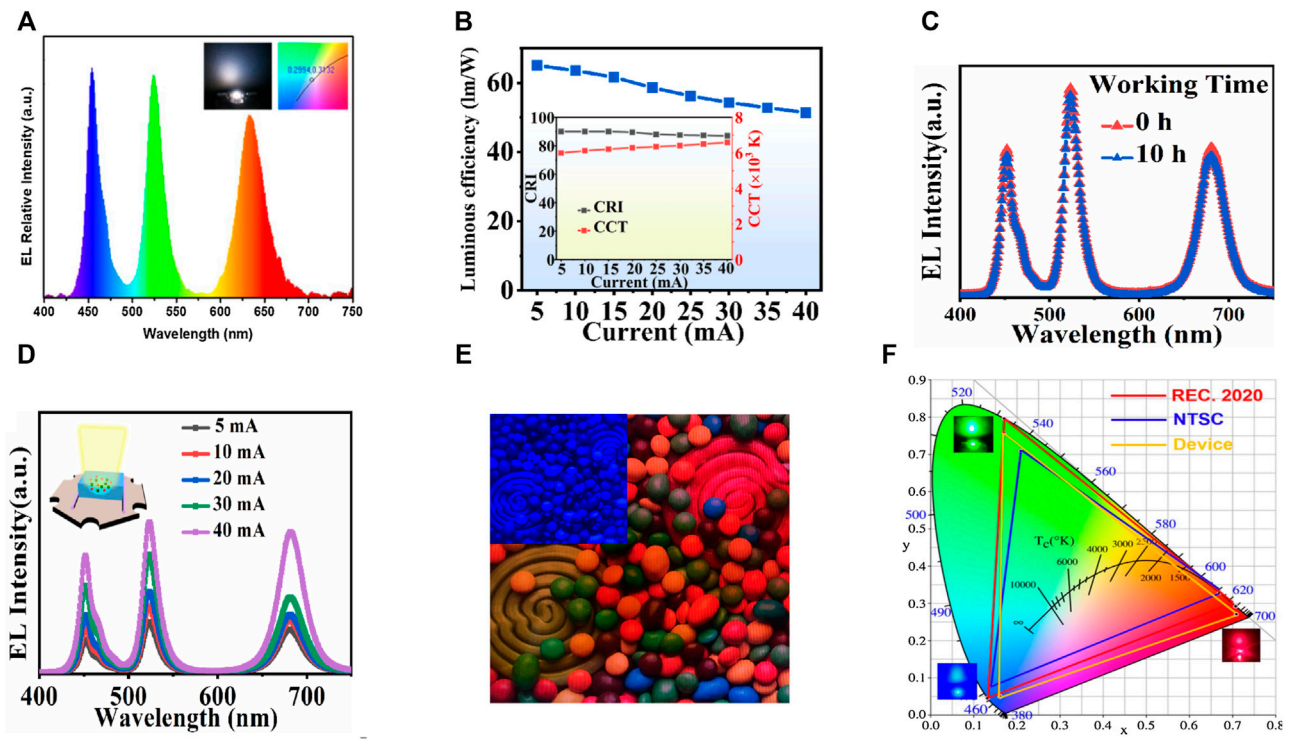

FIGURE 9 | (A) EL spectra of WLEDs obtained by covering a green $CsPbBr_3$ PQD glass sheet coated with red $CsPb(Br/I)_3$ PQD glass powder film on a blue InGaN chip (Inset is the image and CIE of WLED). **(B)** Luminous efficiency of WLED based on $CsPbBr_3$@SiO_2 and $CsPbBr_{0.6}I_{2.4}$@SiO_2 NCs as a function of different driving currents. Inset is the CRI and CCT of the WLED under different driving currents). **(C)** Working stability of the WLED at 5 mA current. **(D)** EL spectra of the WLED with different driving currents. (Inset is the schematic device architecture of the WLED). **(E)** Photographs of $CsPbX_3$@POE-based backlit LCDs (inset is LCDs with blue chip). **(F)** Color gamut of the WLEDs obtained by covering a green $CsPbBr_3$ PQD glass sheet coated with red $CsPb(Br/I)_3$ PQD glasses powder film on a blue InGaN chip in the CIE 1931 color space. **(A,F)** are reproduced with permission from Yang et al. (2022). Copyright 2021, Elsevier Ltd. **(B–D)** are reproduced with permission from Gao et al. (2021). Copyright 2020, Elsevier B.V. **(E)** is reproduced with permission from Mei et al. (2022). Copyright 2022, Elsevier B.V.

TABLE 2 | Chart for different parameters of WLEDs fabricated by embedding green- and red-emitting perovskite NCs upon a blue LED chip.

S.I No	Perovskite material	Synthesis method	CIE color coordinates	CCT (K)	CRI	LE (Lumens/ Watt)	Color gamut (compared to NTSC)	References
1	$CsPbBr_3$ and $CsPbBr_{0.6}I_{2.4}@SiO_2$	LARP	0.32, 0.33	5993–6588	90	65	—	Gao et al. (2021)
2	$CsPbBr_2I$ and $CsPbI_3$@MOF	LARP	0.36, 0.32	—	—	21	125%	Cuan et al. (2021)
3	$CsPbBr_3$ and $CsPb(Br/I)_3$@ borosilicate glass	Melt-quenching	0.2994, 0.3132	—	—	21	121.9%	Yang et al. (2022)
4	$CsPbBr_3$ and $CsPbBrI_2$@ POE	Hot-injection	0.3389,0.3348	—	—	15.72	117%	Mei et al. (2022)

WLEDs, one can also replace these traditional phosphors with perovskites such as green-emitting $CsPbBr_3$ or red-emitting $CsPbI_3$.

Therefore, Gao et al. synthesized $CsPbBr_3$ NCs and assembled them into silica shells to form $CsPbBr_3@SiO_2$ nanocomposites with a high QY of 87% (Gao et al., 2021). The introduction of hydrophobic and multi-branched trioctylphosphine oxide (TOPO), suppressed the rate of hydrolysis of tetraethoxysilane (TEOS). As a result, the anion-exchange reaction among different perovskite-NCs was completely inhibited. A WLED was fabricated by combining $CsPbBr_3@SiO_2$ NCs with $CsPbBr_{0.6}I_{2.4}@SiO_2$ NCs onto blue GaN chips. He obtained a CIE at (0.32, 0.33) at 5 mA current. They also achieved a high CRI of 90 and an LE of 65 Lumens/Watt. The CCT displayed a tunable range of 5993–6588 K with an injection current from 5 to 40 mA (*see* **Figures 9B,D**). To further know about the device stability, **Figure 9C** showed the EL spectra of this WLED before/after a continuous working period of 10 h at 5 mA. No change was seen for the two EL spectra. Similarly, Cuan and his coworkers used a hierarchically porous metal-organic framework grown *in situ* on $CsPbX_3$ perovskite NCs (Cuan et al., 2021). Hierarchically porous MOF enables the impregnation of perovskite precursors in one step and allows more facile diffusion of the reactants. By integrating the green-emitting $CsPbBr_2I$@MOF and red-emitting $CsPbI_3$@MOF nanocomposites with a commercial blue GaN LED chip, a WLED was fabricated, which exhibited white light emission with CIE obtained at (0.36, 0.32). The fabricated WLED demonstrated an LE of 21 Lumens/Watt. They also measured the wide color gamut, which showed an NTSC value of 125% and Rec. 2020 of 93% under a driving current of 20 mA.

Next year, Yang et al. synthesized $CsPbBr_3$-embedded borosilicate glass through melt quenching and *in situ* crystallization using PbO instead of $PbBr_2$ as the lead source (Yang et al., 2022). By adjusting the halogen element, they also synthesized red $CsPb(Br/I)_3$ and blue $CsPb(Br/Cl)_3$ PNC glasses. The WLED was fabricated by combining green $CsPbBr_3$ PNC glass sheet coated with red CsPb(Br/I) PNC glasses powder film on a blue InGaN chip. The WLED had a white light emission (EL spectra are shown in **Figure 9A**) with CIE at (0.2994, 0.3132) (*see* **Figure 9F**) with an LE of 21 Lumens/Watt. The device achieved a wide color gamut of 121.9% NTSC standard and 91.1% Rec. 2020 standard in the CIE 1931 color space. Later, Mei et al. reported the synthesis of green and red $CsPbX_3$ PNCs by encapsulating SiO_2 and POE to protect them from moisture and heat stability (Mei et al., 2022). They obtained $CsPbBr_3$ and $CsPbBrI_2$ PNCs by the hot-injection method. Due to the excellent photoelectric properties of POE-encapsulated PNCs, they fabricated a WLED by combining $CsPbBr_3$@POE and $CsPbBrI_2$@POE composite film with a blue chip. The LE of the fabricated WLED was 15.72 Lumens/Watt with a CIE value of (0.3389, 0.3348). Besides this, the WLED showed a wide color gamut with 117% of the NTSC standard. Next, they demonstrated a liquid crystal (LCD) display by combining green-emitting $CsPbBr_3$@ POE and red-emitting $CsPbBrI_2$ @ POE composite films, as shown in **Figure 9E**. The summary of all the parameters of the fabricated WLEDs by using green- and red-emitting halide perovskites with blue chip is shown in **Table 2**.

UV LED Chip + Metal Halide Perovskite NCs

To fabricate WLED by using a UV LED chip needs three main colors, i.e., blue, green, and red to be excited under UV illumination. Here halide perovskites are major candidates to be used as color conversion layers. These materials cover the entire visible spectrum.

In this context, Zheng et al. reported Mn and Cu co-doping at a different molar concentration to obtain $CsPbCl_{3-x}Br_x$ NCs through anion exchange by $PbBr_2$ at room temperature (Zheng et al., 2020). In this work, they first synthesized Mn and Cu co-doped $CsPbCl_3$. Then they mixed the NC solution with $PbBr_2$ precursor to obtain Mn and Cu co-doped $CsPbCl_{3-x}Br_x$. The incorporation of Cu ions in $CsPbCl_3$ reduced the defect states, resulting in an enhancement in emission due to Mn doping. These Mn and Cu co-doped $CsPbCl_{3-x}Br_x$ NCs show dual blue-orange emission with a QY of 53% and green-emitting NCs, i.e., $CsPbBr_3@Cs_4PbBr_6$ core@ shell with a QY over 90% was used to fabricate a WLED. The emission spectra of WLED fabricated by green $CsPbBr_3@Cs_4PbBr_6$ core@shell and blue-orange co-doped $CsPbCl_{3-x}Br_x$ NCs with the molar ratio of Mn, Pb, and Cu (2/1/2) excited by a 395-nm InGaN UV chip were obtained at 517, 450, and 600 nm, respectively. The improved performance of the WLEDs was controlled by changing the thickness of two emitting layers. The obtained WLED had CRI 85, LE 69%, and CCT 4872 K, and got a CIE value of WLED (0.346, 0.336) operated at a current of 10 mA. Also, they observed that an increase in the intensity of Mn emission improves the CRI of WLEDs. The stability of WLED was also checked with different work times from 0 to 24 h. A significant decrease in emission was observed, which was because WLED was not encapsulated. But it was noted that the emission of dual emitting blue-orange Mn and Cu co-doped $CsPbCl_{3-x}Br_x$ NCs decreases comparatively slower

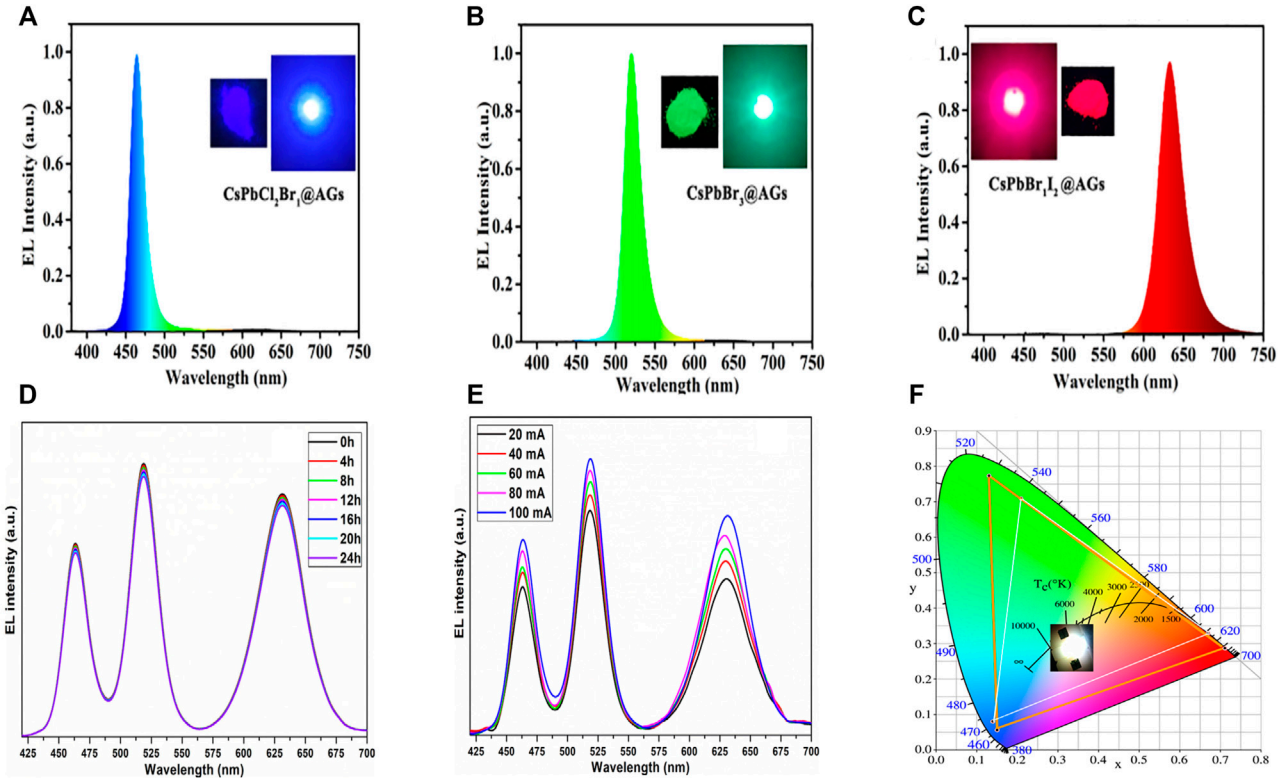

FIGURE 10 | EL spectra of LEDs fabricated from **(A)** $CsPbCl_2Br_1$@AG, **(B)** $CsPbBr_3$@AG, and **(C)** $CsPbBr_1I_2$@AG composites. (Insets: photographic images of corresponding blue, green, and red LED respectively). EL spectra of a constructed WLED based on PNC-encapsulated SiO_2/PMMA operated at **(D)** different time intervals and **(E)** different driving currents. **(F)** CIE chromaticity coordinates, and color gamut of different LEDs fabricated from $CsPbCl_2Br_1$@AG, $CsPbBr_3$@AG, and $CsPbBr_1I_2$@AG composites excited by GaN blue chip. **(A–C,F)** are reproduced with permission from Chen et al. (2022). Copyright 2021, Elsevier B.V. **(D,E)** are reproduced with permission from Naresh et al. (2021). Copyright 2020, Springer-Verlag GmbH.

than green-emitting undoped $CsPbBr_3$ NCs. These results showed that Mn and Cu co-doped $CsPbCl_{3-x}Br_x$ NCs were promising perovskites for fabricating high-quality WLEDs.

In 2021, Chen et al. reported Mn-doped lead halide $CsPb(Br/Cl)_3$ as a promising phosphor material for fabricating WLEDs (Chen et al., 2021c). The obtained perovskites showed dual-color emission with blue emission at 463 nm and red emission at 602 nm. They fabricated two kinds of WLED, including the single-component Mn-doped $CsPb(Br/Cl)_3$ phosphor-based WLED and the dual-component $CsPbBr_3$/Mn-doped $CsPb(Br/Cl)_3$ mixture phosphors. The prototypes were fabricated by coating as-prepared phosphors/silicone gel mixture on UV InGaN LED chips. The EL spectra of single-component WLED exhibited strong orange-red emission and relatively weak blue emission, which had no significant change when the driving current is increased from 30 to 150 mA. The warm light had been obtained at a driving current of 30 mA. But the dual-component WLED contained blue, green, and red PL peaks, which are at 426, 520, and 609 nm, respectively. The CIE obtained was (0.39, 0.38).

Similarly, Naresh et al. reported the blue-green-red emitting $CsPbX_3$ (X = Cl/Br, Br, Br/I) PNC synthesis *via* the hot-injection method. Later they coated with silica and embedded in poly(methylmethacrylate) (PMMA) matrix (Naresh et al., 2021). The QYs of blue, green, and red-emitting SiO_2/PMMA-coated PNCs were 37, 86, and 71%, respectively. Furthermore, the PNC-encapsulated SiO_2/PMMA composite films were coupled on the surface of 365 nm UV LED to achieve white light emission. The designed WLED device was operated at 20 mA current. The obtained white light has CIE of (0.349, 0.350) and LE of 39.2%. A CCT of 4825 K and a CRI of 84.7 were achieved. They also performed the stability of fabricated WLED, which showed tremendous resilience up to 24 h at 20 mA driving current (*see* **Figure 10D**). There was no spectral variation observed in the EL spectra. The constructed WLED also exhibited EL spectra by increasing the current flow from 20 to 100 mA (*see* **Figure 10E**). Additionally, the device produced a wide color gamut of 121.47% of NTSC and 98.56% of Rec. 2020 in CIE 1931 color space.

As another example, Lu et al. synthesized $CsPbBr_{1.5}I_{1.5}$ NCs and grew them *in situ* on SrHAp [strontium hydroxyphosphate, $Sr_5(PO_4)_3OH$] nanorods (Lu et al., 2021). The $CsPbBr_{1.5}I_{1.5}$@SrHAp samples showed both the intrinsic luminescence from the matrix and the emission of $CsPbBr_{1.5}I_{1.5}$ PNCs, which result in the tunable multi-color emissions in a single-phase phosphor by changing the amounts of SrHAp matrix or adjusting the excitation wavelengths. The corresponding WLED had white

TABLE 3 | Chart for different parameters of WLEDs fabricated by embedding green, red, and blue-emitting perovskite NCs upon a UV LED chip.

S.I. No	Perovskite material	Synthesis method	CIE color coordinates	CCT (K)	CRI	LE (Lumens/ Watt)	Color gamut (compared to NTSC)	Reference
1	Mn and Cu co-doped $CsPbCl_{3-x}Br_x$ and $CsPbBr_3$@ Cs_4PbBr_6	Hot-injection	0.346, 0.336	4872	85	69	—	Zheng et al. (2020)
2	Mn-doped $CsPb(Br/Cl)_3$ and $CsPbBr_3$@SiO_2	Hot-injection	0.39, 0.38	—	—	—	—	Chen et al. (2021c)
3	$CsPbX_3$@SiO_2/PMMA	Hot-injection	—	4825	84.7	—	121.47%	Naresh et al. (2021)
4	$CsPbBr_{1.5}I_{1.5}$@SrHAp	Hot-injection	0.343, 0.313	4905	91.8	17.8	—	Lu et al. (2021)
5	$CsPbCl_2Br1$, $CsPbBr_3$, and $CsPbBr_1I_2$@SiO_2 AGs	Hot-injection	0.3010, 0.3108	5834	86.7	79.53	—	Chen et al. (2022)
6	$CsPbBr_3/Nd^{3+}$	Hot-injection	0.32, 0.34	—	—	—	—	Padhiar et al. (2022)
7	CPB-20°C, CPB- 80°C, Mn-doped PEA_2PbBr_4	—	—	—	96	—	—	Sun et al. (2022)
8	$CsPb(Cl/Br)_3$, $CsPbBr_3$, and Mn:Cs_4PbCl_6	Hot-injection	0.3229, 0.3037	5586	—	—	—	Shi et al. (2022)

light emission with the chromaticity coordinates (0.343, 0.313), a CCT of 4905 K, a CRI of 91.8, and an LE of 17.8 Lumens/Watt, respectively.

Later, Z. Chen et al. encapsulated $CsPbX_3$ (X = Cl, Br, I) PNCs are encapsulated into super-hydrophobic silica aerogels (SiO_2 AGs) to form a protective layer for resisting destruction by external forces (Chen et al., 2022). The $CsPbCl_2Br_1$@AG, $CsPbBr_3$@AG, and $CsPbBr_1I_2$@AG composites were synthesized with narrow emissions that replaced traditional phosphors as color converters. Stable white light emission is generated by two ways i.e., coupling separate $CsPbBr_3$@AG/ $CsPbBr_1I_2$@AG (WLED-1) or coupling YAG: Ce^{3+}/$CsPbBr_1I_2$@ AG (WLED-2) composites on GaN blue chip. As shown in **Figures 10A–C**, the EL spectra of $CsPbCl_2Br_1$@AG, $CsPbBr_3$@ AG, and $CsPbBr_1I_2$@AG composites powders emitting blue, green, and red light can be excited by the GaN blue chip. The fabricated WLED-1 had a LE of 14.55 Lumens/Watt, R_a of 94.9, and CCT of 5477 K, while the WLED-2 had an LE of 79.53 Lumens/Watt, CCT 5834 K, and R_a of 86.7, respectively. Finally, $CsPbX_3$@AG@PS composite film based on dual protection of aerogel and PS polymer, the composite film achieved CIE of (0.3010, 0.3108) as shown in **Figure 10F**.

Again, Padhiar et al. reported the change in optical properties of $CsPbBr_3$ NCs by mixing Nd^{3+} trivalent lanthanide halide cations (Padhiar et al., 2022). The Nd^{3+} cations, when incorporated into $CsPbBr_3$ NCs, reduced the nonradiative recombination more efficiently. As a result of this, the PL QY has been significantly increased to 91%. A WLED device was fabricated using the $CsPbBr_3/Nd^{3+}$ NCs integrated with an ultraviolet (UV) LED chip, producing a cool white light emission with a CIE value at (0.32, 0.34). Furthermore, Sun et al. performed the synthesis of three-color perovskite phosphors, i.e., blue-emitting $CsPbBr_3$ NCs synthesized at 20°C, green-emitting $CsPbBr_3$ NCs synthesized at 80°C, and red-emitting Mn-doped PEA_2PbBr_4 NCs were coupled together to generate warm white light emission with a CRI value of 96 (Sun et al., 2022).

In addition to those, Shi et al. synthesized 0D-Cs_4PbX_6 NCs and adjusted the bandgap *via* Mn doping (Mn:Cs_4PbX_6) (Shi et al., 2022). $CsPb(Cl/Br)_3$, $CsPbBr_3$, and Mn:Cs_4PbCl_6 NCs were mixed in a toluene solution of PS to prepare blue, green, and red luminescent films, respectively. The WLED device was designed by placing the films as color conversion layers above a 280-nm LED chip. The color coordinates of the white LED in the CIE chromaticity diagram are (0.3229, 0.3037), which are located in the white area with a CCT of 5586 K. The summary of all the parameters of the fabricated WLEDs by using red, green, and blue-emitting halide perovskites embedded on a UV LED chip is shown in **Table 3**.

CONCLUDING REMARKS AND PERSPECTIVES

This review basically emphasizes the current research progress and the potential of perovskite conversion layer in WLEDs. The WLEDs highly require energy efficiency, high CRI, easily tunable CCT, high luminous intensity, but at the same time need to be cost-effective suitable for their production at a large scale. In the last two decades, many phosphors have been investigated regarding WLEDs, which are currently going to reach the saturation point in terms of having new alternate phosphors and lack of optimization in the recent ones. Also, the PL QY of the phosphor-converted WLED system is low and CCT is quite high, resulting in bluish or cool WLED. By replacing the conventional phosphors with perovskite NCs, the CCT value can be optimized to a lower possible forming a natural white light. However, their instability against various environmental factors, such as humidity, temperature, light, and polar solvents, still remains an issue. On the other hand, the optical properties of these perovskite materials need to be taken care of, or the minimized optical loss has to be controlled during the integration of these materials into polymers such as silicone resin. One of the various strategies is to encapsulate the

perovskite NCs with suitable metal oxides, lower dimensional perovskites, MOFs, long chained polymers, etc., which increase their stability and optical properties. As a result, these composites show great potential as color conversion layers for WLEDs, making them extra durable and efficient at the same time. For obtaining a decent WLED, a CIE value of (0.33, 0.33), a CRI value of nearly 80, and an LE in the range of 20–60 Lumens/Watt are necessary. It can also be observed that emission intensity while operation of WLEDs increases at high currents leads to excess heating that degrades the NC conversion layers. Therefore, the device fabrication method should be in such a way that it will deliver a maximum output at even low currents. This can reduce the overheating of WLEDs and prevent the degradation of emitting layers from degradation, overall increasing the working periods of WLEDs. The stability of perovskite NCs against the halide exchange process also proves their potential capability in lithography (Huang et al., 2020). The top-down lithographic method combining photolithography, electron-beam lithography, O_2 plasma etching, and argon milling can be applied to construct multi-color patterned perovskite films layer by layer, thereby taking efficient WLED from perovskite conversion layers one step further. This paves the way for high-quality flat display technologies.

We also studied the synthesis process of various metal halide perovskite NCs and their subsequent use for WLED applications. The LARP synthetic procedure is one of the most favored synthetic protocols for perovskite NCs because it is a very facile and cost-effective RT process that allows large-scale production to yield high-quality perovskite NCs. The stability of perovskites NCs, precisely the heat stability, and stability against halide exchange are some of the prime aspects for producing efficient WLEDs working for longer periods of time. Compared with organic–inorganic hybrid perovskites, including large organic cations like MA or FA, the heat stability is found to be better for all inorganic perovskites, mostly for Cs-based perovskites, which is also a reason that $CsPbX_3$ perovskite NCs are mainly used as color converters (Li et al., 2019). Furthermore, the encapsulation also inhibits halide exchange between NCs containing different halide anions (Gao et al., 2021). Another aspect is the widely tunable bandgap of these NCs, which covers most of the visible spectrum region, and the PL spectra generally have high color purity and narrow FWHM (Protesescu et al., 2015). As a result, mixing different perovskites emitting in the blue, green, or red region for white light emission would be effective. On the other hand, encapsulation of perovskite NCs in polymer matrices also results in highly flexible films, which are beneficial for future display technologies (Tang et al., 2021). These properties open ways for a more efficient combination of colors to obtain a perfect white ligiht emission closer to CIE color coordinates (0.33, 0.33), a CRI value of 96, and an LE of 101.27 Lumens/Watt. The lead-halide perovskite WLEDs are facing the toxicity issue for the Pb element present inside the perovskite structure which causes health and environmental issues (Ke and Kanatzidis, 2019; Ning and Gao, 2019; Zhang et al., 2019). Use of nontoxic lead-free perovskites as conversion layers can tackle such an issue. Interestingly, lead-free perovskites have improved thermodynamic and chemical stability which makes them potential candidates for future lead-free WLEDs. However, the emission QY and stability of lead-free perovskite NCs are still not comparable to lead-based perovskite materials, preventing the development of high-performance LEDs. Many efforts are required for the improvement of the emission properties of lead-free perovskites that can have superior optical properties that can replace lead-based perovskite materials for LEDs.

AUTHOR CONTRIBUTIONS

All authors equally contributed to writing the manuscript.

ACKNOWLEDGMENTS

SB acknowledges to Department of Science and Technology (DST), India (Award number# DST/INSPIRE/04/2017/000530), and Science and Engineering Research Board (SERB), India (Award number# SRG/2019/000093), for financial support.

REFERENCES

Ahmed, G. H., Yin, J., Bakr, O. M., and Mohammed, O. F. (2021). Successes and Challenges of Core/Shell Lead Halide Perovskite Nanocrystals. *ACS Energ. Lett.* 6, 1340–1357. doi:10.1021/acsenergylett.1c00076

Akkerman, Q. A., D'Innocenzo, V., Accornero, S., Scarpellini, A., Petrozza, A., Prato, M., et al. (2015). Tuning the Optical Properties of Cesium Lead Halide Perovskite Nanocrystals by Anion Exchange Reactions. *J. Am. Chem. Soc.* 137, 10276–10281. doi:10.1021/jacs.5b05602

Akkerman, Q. A., Rainò, G., Kovalenko, M. V., and Manna, L. (2018). Genesis, Challenges and Opportunities for Colloidal lead Halide Perovskite Nanocrystals. *Nat. Mater* 17, 394–405. doi:10.1038/s41563-018-0018-4

Baekelant, W., Coutino-Gonzalez, E., Steele, J. A., Roeffaers, M. B. J., and Hofkens, J. (2017). Form Follows Function: Warming White LEDs Using Metal Cluster-Loaded Zeolites as Phosphors. *ACS Energ. Lett.* 2, 2491–2497. doi:10.1021/acsenergylett.7b00765

Baranov, D., Fieramosca, A., Yang, R. X., Polimeno, L., Lerario, G., Toso, S., et al. (2021). Aging of Self-Assembled Lead Halide Perovskite Nanocrystal Superlattices: Effects on Photoluminescence and Energy Transfer. *ACS Nano* 15, 650–664. doi:10.1021/acsnano.0c06595

Bhaumik, S. (2019). Oriented Attachment of Perovskite Cesium Lead Bromide Nanocrystals. *ChemistrySelect* 4, 4538–4543. doi:10.1002/slct.201900142

Bhaumik, S., Veldhuis, S. A., Ng, Y. F., Li, M., Muduli, S. K., Sum, T. C., et al. (2016). Highly Stable, Luminescent Core-Shell Type Methylammonium-Octylammonium lead Bromide Layered Perovskite Nanoparticles. *Chem. Commun.* 52, 7118–7121. doi:10.1039/c6cc01056c

Boles, M. A., Ling, D., Hyeon, T., and Talapin, D. V. (2016). The Surface Science of Nanocrystals. *Nat. Mater* 15, 141–153. doi:10.1038/nmat4526

Burda, C., Chen, X., Narayanan, R., and El-Sayed, M. A. (2005). Chemistry and Properties of Nanocrystals of Different Shapes. *Chem. Rev.* 105, 1025–1102. doi:10.1021/cr030063a

Chen, C., Zhang, L., Shi, T., Liao, G., and Tang, Z. (2019). Controllable Synthesis of All Inorganic Lead Halide Perovskite Nanocrystals with Various Appearances in Multiligand Reaction System. *Nanomaterials* 9, 1751. doi:10.3390/nano9121751

Chen, R., Xu, Y., Wang, S., Xia, C., Liu, Y., Yu, B., et al. (2021). Zinc Ions Doped Cesium lead Bromide Perovskite Nanocrystals with Enhanced Efficiency and

Stability for white Light-Emitting Diodes. *J. Alloys Compd.* 866, 158969. doi:10.1016/j.jallcom.2021.158969

Chen, Z., He, H., Wen, Z., Cui, Z., Mei, S., Yang, D., et al. (2021). Highly Efficient Mn-Doped CsPb(Br/Cl)$_3$ Mixed-Halide Perovskite via a Simple Large-Scale Synthesis Method. *Mater. Sci. Eng. B* 273, 115426. doi:10.1016/j.mseb.2021.115426

Chen, Z., Mei, S., He, H., Wen, Z., Cui, Z., Yang, B., et al. (2021). Rapid Large-Scale Synthesis of Highly Emissive Solid-State Metal Halide Perovskite Quantum Dots across the Full Visible Spectrum. *Opt. Laser Technol.* 143, 107369. doi:10.1016/j.optlastec.2021.107369

Chen, Z., Zhao, J., Zeng, R., Liu, X., Zou, B., and Xiang, W. (2022). High Efficiency Fluorescent Perovskite Quantum Dots Encapsulated in Superhydrophobic Silica Aerogel for Wide Color Gamut Backlight Displays. *Chem. Eng. J.* 433, 133195. doi:10.1016/j.cej.2021.133195

Correa-Baena, J.-P., Abate, A., Saliba, M., Tress, W., Jesper Jacobsson, T., Grätzel, M., et al. (2017). The Rapid Evolution of Highly Efficient Perovskite Solar Cells. *Energy Environ. Sci.* 10, 710–727. doi:10.1039/c6ee03397k

Crawford, M. H. (2009). LEDs for Solid-State Lighting: Performance Challenges and Recent Advances. *IEEE J. Select. Top. Quan. Electron.* 15, 1028–1040. doi:10.1109/jstqe.2009.2013476

Cuan, J., Zhang, D., Xing, W., Han, J., Zhou, H., and Zhou, Y. (2021). Confining $CsPbX_3$ Perovskites in a Hierarchically Porous MOF as Efficient and Stable Phosphors for white LED. *Chem. Eng. J.* 425, 131556. doi:10.1016/j.cej.2021.131556

D'Andrade, B. W., and Forrest, S. R. (2004). White Organic Light-Emitting Devices for Solid-State Lighting. *Adv. Mater.* 16, 1585–1595. doi:10.1002/adma.200400684

Dai, Q., Duty, C. E., and Hu, M. Z. (2010). Semiconductor-Nanocrystals-Based White Light-Emitting Diodes. *Small* 6, 1577–1588. doi:10.1002/smll.201000144

Dongdong, Y., Shuangyi, Z., Yubo, Z., Huaxin, W., and Zhigang, Z. (2022). Highly Efficient Emission and High-CRI Warm white Light-Emitting Diodes from Ligand-Modified $CsPbBr_3$ Quantum Dots. *Opto-Electron Adv.* 5, 200075. doi:10.29026/oea.2022.200075

Dou, B., Du, W., Huang, F., Ma, H., Hua, Y., Zhang, J., et al. (2020). A Next-Generation Wide Color Gamut WLED with Improved Spectral Performance in Phosphor Composite Functional Solid. *Ceramics Int.* 46, 27126–27133. doi:10.1016/j.ceramint.2020.07.190

Du, K., He, L., Song, S., Feng, J., Li, Y., Zhang, M., et al. (2021). *In Situ* Embedding Synthesis of Highly Stable $CsPbBr_3/CsPb_2Br_5$ @PbBr(OH) Nano/Microspheres through Water Assisted Strategy. *Adv. Funct. Mater.* 31, 2103275. doi:10.1002/adfm.202103275

Fang, Z., Wu, K., Wang, L., Xu, D., Wang, W., Lin, Y., et al. (2021). Highly Efficient and Blue-Excitable Mn-Doped PEA2Pb(Br/I)4 Perovskite for Solid Lighting. *J. Lumin.* 237, 118155. doi:10.1016/j.jlumin.2021.118155

Gao, F., Yang, W., Liu, X., Li, Y., Liu, W., Xu, H., et al. (2021). Highly Stable and Luminescent Silica-Coated Perovskite Quantum Dots at Nanoscale-Particle Level via Nonpolar Solvent Synthesis. *Chem. Eng. J.* 407, 128001. doi:10.1016/j.cej.2020.128001

García de Arquer, F. P., Armin, A., Meredith, P., and Sargent, E. H. (2017). Solution-processed Semiconductors for Next-Generation Photodetectors. *Nat. Rev. Mater.* 2, 16100. doi:10.1038/natrevmats.2016.100

Huang, G., Huang, Y., Xu, W., Yao, Q., Liu, X., Ding, C., et al. (2019). Cesium lead Halide Perovskite Nanocrystals for Ultraviolet and Blue Light Blocking. *Chin. Chem. Lett.* 30, 1021–1023. doi:10.1016/j.cclet.2018.12.028

Huang, X., Xiao, X., and Dong, G. (2020). Metal Halide Perovskites Functionalized by Patterning Technologies. *Adv. Mater. Technol.* 5, 2000513. doi:10.1002/admt.202000513

Jia, C., Li, H., Meng, X., and Li, H. (2018). $CsPbX_3/Cs_4PbX_6$ Core/shell Perovskite Nanocrystals. *Chem. Commun.* 54, 6300–6303. doi:10.1039/c8cc02802h

Kamat, P. V., Pradhan, N., Schanze, K., Weiss, P. S., Buriak, J., Stang, P., et al. (2020). Challenges and Opportunities in Designing Perovskite Nanocrystal Heterostructures. *ACS Energ. Lett.* 5, 2253–2255. doi:10.1021/acsenergylett.0c01216

Kar, M. R., Ray, S., Patra, B. K., and Bhaumik, S. (2021). State of the Art and Prospects of Metal Halide Perovskite Core@shell Nanocrystals and Nanocomposites. *Mater. Today Chem.* 20, 100424. doi:10.1016/j.mtchem.2021.100424

Kazes, M., Udayabhaskararao, T., Dey, S., and Oron, D. (2021). Effect of Surface Ligands in Perovskite Nanocrystals: Extending in and Reaching Out. *Acc. Chem. Res.* 54, 1409–1418. doi:10.1021/acs.accounts.0c00712

Ke, W., and Kanatzidis, M. G. (2019). Prospects for Low-Toxicity lead-free Perovskite Solar Cells. *Nat. Commun.* 10, 965. doi:10.1038/s41467-019-08918-3

Kong, Z.-C., Liao, J.-F., Dong, Y.-J., Xu, Y.-F., Chen, H.-Y., Kuang, D.-B., et al. (2018). Core@Shell $CsPbBr_3$@Zeolitic Imidazolate Framework Nanocomposite for Efficient Photocatalytic CO_2 Reduction. *ACS Energ. Lett.* 3, 2656–2662. doi:10.1021/acsenergylett.8b01658

Kovalenko, M. V., Protesescu, L., and Bodnarchuk, M. I. (2017). Properties and Potential Optoelectronic Applications of lead Halide Perovskite Nanocrystals. *Science* 358, 745–750. doi:10.1126/science.aam7093

Kramer, I. J., and Sargent, E. H. (2014). The Architecture of Colloidal Quantum Dot Solar Cells: Materials to Devices. *Chem. Rev.* 114, 863–882. doi:10.1021/cr400299t

Krames, M. R., Shchekin, O. B., Mueller-Mach, R., Mueller, G. O., Zhou, L., Harbers, G., et al. (2007). Status and Future of High-Power Light-Emitting Diodes for Solid-State Lighting. *J. Display Technol.* 3, 160–175. doi:10.1109/jdt.2007.895339

Li, X., Tan, Y., Lai, H., Li, S., Chen, Y., Li, S., et al. (2019). All-Inorganic $CsPbBr_3$ Perovskite Solar Cells with 10.45% Efficiency by Evaporation-Assisted Deposition and Setting Intermediate Energy Levels. *ACS Appl. Mater. Inter.* 11, 29746–29752. doi:10.1021/acsami.9b06356

Li, X., Cai, W., Guan, H., Zhao, S., Cao, S., Chen, C., et al. (2021). Highly Stable $CsPbBr_3$ Quantum Dots by Silica-Coating and Ligand Modification for white Light-Emitting Diodes and Visible Light Communication. *Chem. Eng. J.* 419, 129551. doi:10.1016/j.cej.2021.129551

Li, X., Cao, F., Yu, D., Chen, J., Sun, Z., Shen, Y., et al. (2017). All Inorganic Halide Perovskites Nanosystem: Synthesis, Structural Features, Optical Properties and Optoelectronic Applications. *Small* 13, 1603996. doi:10.1002/smll.201603996

Li, X., Wei, Y., Dang, P., Xiao, X., Xiao, H., Zhang, G., et al. (2022). Enhancing the Stability of Perovskite Quantum Dots CsPbX3 (X=Cl, Br, I) by Encapsulation in Porous Y_2O_3 Nanoparticles for WLED Applications. *Mater. Res. Bull.* 146, 111592. doi:10.1016/j.materresbull.2021.111592

Li, Y., Zhang, X., Huang, H., Kershaw, S. V., and Rogach, A. L. (2020). Advances in Metal Halide Perovskite Nanocrystals: Synthetic Strategies, Growth Mechanisms, and Optoelectronic Applications. *Mater. Today* 32, 204–221. doi:10.1016/j.mattod.2019.06.007

Li, Z. J., Hofman, E., Li, J., Davis, A. H., Tung, C. H., Wu, L. Z., et al. (2018). Photoelectrochemically Active and Environmentally Stable $CsPbBr_3/TiO_2$ Core/Shell Nanocrystals. *Adv. Funct. Mater.* 28, 1704288. doi:10.1002/adfm.201704288

Li, Z., Zhou, F., Yao, H., Ci, Z., Yang, Z., and Jin, Z. (2021). Halide Perovskites for High-Performance X-ray Detector. *Mater. Today* 48, 155–175. doi:10.1016/j.mattod.2021.01.028

Lin, C. C., Meijerink, A., and Liu, R.-S. (2016). Critical Red Components for Next-Generation White LEDs. *J. Phys. Chem. Lett.* 7, 495–503. doi:10.1021/acs.jpclett.5b02433

Liu, M., Yazdani, N., Yarema, M., Jansen, M., Wood, V., and Sargent, E. H. (2021). Colloidal Quantum Dot Electronics. *Nat. Electron.* 4, 548–558. doi:10.1038/s41928-021-00632-7

Lu, Y., Zhang, C., Yuan, S., Zhang, C., Wang, J., Kong, H., et al. (2021). Novel $CsPbBr_{1.5}I_{1.5}$@SrHAp Single-phase white-light Emitting Phosphors: Facile Synthesis, Formation Process, Enhanced Stability, and Color-Tunable Luminescence. *Chem. Eng. J.* 426, 130809. doi:10.1016/j.cej.2021.130809

Mei, E., Li, J., He, Q., Tong, Y., Liu, R., Fan, H., et al. (2022). POE Enhanced Stabilities of CsPbX3 (X = Br, I) Perovskite and Their white LED Application. *J. Energ. Chem.* 67, 193–200. doi:10.1016/j.jechem.2021.10.005

Mondal, R. K., Adhikari, S., Chatterjee, V., and Pal, S. (2021). Recent Advances and Challenges in AlGaN-Based Ultra-violet Light Emitting Diode Technologies. *Mater. Res. Bull.* 140, 111258. doi:10.1016/j.materresbull.2021.111258

Nakamura, S., Mukai, T., and Senoh, M. (1994). Candela-class High-brightness InGaN/A_lGaN Double-heterostructure Blue-light-emitting Diodes. *Appl. Phys. Lett.* 64, 1687–1689. doi:10.1063/1.111832

Nakamura, S., Mukai, T., and Senoh, M. (1994). High-brightness InGaN/AlGaN Double-heterostructure blue-green-light-emitting Diodes. *J. Appl. Phys.* 76, 8189–8191. doi:10.1063/1.357872

Nakamura, S., Senoh, M., and Mukai, T. (1993). High-power InGaN/GaN Double-heterostructure Violet Light Emitting Diodes. *Appl. Phys. Lett.* 62, 2390–2392. doi:10.1063/1.109374

Nardelli, A., Deuschle, E., de Azevedo, L. D., Pessoa, J. L. N., and Ghisi, E. (2017). Assessment of Light Emitting Diodes Technology for General Lighting: A Critical Review. *Renew. Sustain. Energ. Rev.* 75, 368–379. doi:10.1016/j.rser.2016.11.002

Naresh, V., Kim, B. H., and Lee, N. (2021). Synthesis of $CsPbX_3$ (X = Cl/Br, Br, and Br/I)@SiO_2/PMMA Composite Films as Color-Conversion Materials for Achieving Tunable Multi-Color and white Light Emission. *Nano Res.* 14, 1187–1194. doi:10.1007/s12274-020-3170-5

Nedelcu, G., Protesescu, L., Yakunin, S., Bodnarchuk, M. I., Grotevent, M. J., and Kovalenko, M. V. (2015). Fast Anion-Exchange in Highly Luminescent Nanocrystals of Cesium Lead Halide Perovskites ($CsPbX_3$, X = Cl, Br, I). *Nano Lett.* 15, 5635–5640. doi:10.1021/acs.nanolett.5b02404

Ning, W., and Gao, F. (2019). Structural and Functional Diversity in Lead-Free Halide Perovskite Materials. *Adv. Mater.* 31, 1900326. doi:10.1002/adma.201900326

Padhiar, M. A., Wang, M., Ji, Y., Yang, Z., and Bhatti, A. S. (2022). Tuning Optical Properties of CsPbBr3 by Mixing Nd3+ Trivalent Lanthanide Halide Cations for Blue Light Emitting Devices. *Nanotechnology* 33, 175202. doi:10.1088/1361-6528/ac4b2e

Pan, A., He, B., Fan, X., Liu, Z., Urban, J. J., Alivisatos, A. P., et al. (2016). Insight into the Ligand-Mediated Synthesis of Colloidal CsPbBr3 Perovskite Nanocrystals: The Role of Organic Acid, Base, and Cesium Precursors. *ACS Nano* 10, 7943–7954. doi:10.1021/acsnano.6b03863

Park, B. w., and Seok, S. I. (2019). Intrinsic Instability of Inorganic-Organic Hybrid Halide Perovskite Materials. *Adv. Mater.* 31, 1805337. doi:10.1002/adma.201805337

Phillips, J. M., Coltrin, M. E., Crawford, M. H., Fischer, A. J., Krames, M. R., Mueller-Mach, R., et al. (2007). Research Challenges to Ultra-efficient Inorganic Solid-State Lighting. *Laser Photon. Rev.* 1, 307–333. doi:10.1002/lpor.200710019

Protesescu, L., Yakunin, S., Bodnarchuk, M. I., Bertolotti, F., Masciocchi, N., Guagliardi, A., et al. (2016). Monodisperse Formamidinium Lead Bromide Nanocrystals with Bright and Stable Green Photoluminescence. *J. Am. Chem. Soc.* 138, 14202–14205. doi:10.1021/jacs.6b08900

Protesescu, L., Yakunin, S., Bodnarchuk, M. I., Krieg, F., Caputo, R., Hendon, C. H., et al. (2015). Nanocrystals of Cesium Lead Halide Perovskites ($CsPbX_3$, X = Cl, Br, and I): Novel Optoelectronic Materials Showing Bright Emission with Wide Color Gamut. *Nano Lett.* 15, 3692–3696. doi:10.1021/nl5048779

Qi, F., Shao, X., Ma, Y., Sun, Y., Zhu, J., Yin, P., et al. (2022). Improved Luminescent Performances of CsPbI3 Perovskite Quantum Dots via Optimizing the Proportion of boron-silicate Glass and Precipitation Processing. *Opt. Mater.* 124, 111981. doi:10.1016/j.optmat.2022.111981

Raja, S. N., Bekenstein, Y., Koc, M. A., Fischer, S., Zhang, D., Lin, L., et al. (2016). Encapsulation of Perovskite Nanocrystals into Macroscale Polymer Matrices: Enhanced Stability and Polarization. *ACS Appl. Mater. Inter.* 8, 35523–35533. doi:10.1021/acsami.6b09443

Roduner, E. (2006). Size Matters: Why Nanomaterials Are Different. *Chem. Soc. Rev.* 35, 583–592. doi:10.1039/b502142c

Sasabe, H., and Kido, J. (2011). Multifunctional Materials in High-Performance OLEDs: Challenges for Solid-State Lighting. *Chem. Mater.* 23, 621–630. doi:10.1021/cm1024052

Schmidt, L. C., Pertegás, A., González-Carrero, S., Malinkiewicz, O., Agouram, S., Mínguez Espallargas, G., et al. (2014). Nontemplate Synthesis of $CH_3NH_3PbBr_3$ Perovskite Nanoparticles. *J. Am. Chem. Soc.* 136, 850–853. doi:10.1021/ja4109209

Schubert, E. F., and Kim, J. K. (2005). Solid-State Light Sources Getting Smart. *Science* 308, 1274–1278. doi:10.1126/science.1108712

Shen, Y., Tang, H., Liu, F., Lin, K., Lu, J., Yan, C., et al. (2021). Stable Cyan and white Light-Emitting Diodes Enabled by Branched Cations Sterically Stabilized 2D/3D Perovskites. *Chem. Eng. J.* 423, 130160. doi:10.1016/j.cej.2021.130160

Shi, W., Zhang, X., Matras-Postolek, K., and Yang, P. (2022). Mn-derived Cs4PbX6 Nanocrystals with Stable and Tunable Wide Luminescence for white Light-Emitting Diodes. *J. Mater. Chem. C* 10, 3886–3893. doi:10.1039/d2tc00014h

Shirasaki, Y., Supran, G. J., Bawendi, M. G., and Bulović, V. (2013). Emergence of Colloidal Quantum-Dot Light-Emitting Technologies. *Nat. Photon* 7, 13–23. doi:10.1038/nphoton.2012.328

Shu, B., Chang, Y., Dong, L., Chen, L., Wang, H., Yang, S., et al. (2021). Highly Stable $CsPbBr_3$ Perovskite Quantum Dots Incorporated in Aluminum Stearate. *J. Lumin.* 234, 117962. doi:10.1016/j.jlumin.2021.117962

Sum, T. C., and Mathews, N. (2014). Advancements in Perovskite Solar Cells: Photophysics behind the Photovoltaics. *Energ. Environ. Sci.* 7, 2518–2534. doi:10.1039/c4ee00673a

Sun, S., Yuan, D., Xu, Y., Wang, A., and Deng, Z. (2016). Ligand-Mediated Synthesis of Shape-Controlled Cesium Lead Halide Perovskite Nanocrystals via Reprecipitation Process at Room Temperature. *ACS Nano* 10, 3648–3657. doi:10.1021/acsnano.5b08193

Sun, Y., Li, Y., Zhang, W., Zhu, P., Zhu, H., Qin, W., et al. (2022). Simultaneous Synthesis, Modification, and DFT Calculation of Three-Color Lead Halide Perovskite Phosphors for Improving Stability and Luminous Efficiency of WLEDs. *Adv. Opt. Mater.* 10, 2101765. doi:10.1002/adom.202101765

Tang, X., Kothalawala, N. L., Zhang, Y., Qian, D., Kim, D. Y., and Yang, F. (2021). Water-driven CsPbBr3 Nanocrystals and Poly(methyl Methacrylate)-$CsPbBr_3$ Nanocrystal Films with Bending-Endurable Photoluminescence. *Chem. Eng. J.* 425, 131456. doi:10.1016/j.cej.2021.131456

Tang, Y., He, X., Zhang, Y., Yuan, H., Xin, Y., Ren, X., et al. (2022). Anchoring of Red Perovskite Nanocrystals on YAG:Ce Phosphor for High Color Rendering index WLEDs. *J. Alloys Compd.* 899, 163347. doi:10.1016/j.jallcom.2021.163347

Tsao, J. Y., Saunders, H. D., Creighton, J. R., Coltrin, M. E., and Simmons, J. A. (2010). Solid-state Lighting: an Energy-Economics Perspective. *J. Phys. D: Appl. Phys.* 43, 354001. doi:10.1088/0022-3727/43/35/354001

Veldhuis, S. A., Boix, P. P., Yantara, N., Li, M., Sum, T. C., Mathews, N., et al. (2016). Perovskite Materials for Light-Emitting Diodes and Lasers. *Adv. Mater.* 28, 6804–6834. doi:10.1002/adma.201600669

Wang, L., Xie, R.-J., Suehiro, T., Takeda, T., and Hirosaki, N. (2018). Down-Conversion Nitride Materials for Solid State Lighting: Recent Advances and Perspectives. *Chem. Rev.* 118, 1951–2009. doi:10.1021/acs.chemrev.7b00284

Wang, S., Bi, C., Yuan, J., Zhang, L., and Tian, J. (2018). Original Core–Shell Structure of Cubic $CsPbBr_3$@Amorphous CsPbBrx Perovskite Quantum Dots with a High Blue Photoluminescence Quantum Yield of over 80. *ACS Energ. Lett.* 3, 245. doi:10.1021/acsenergylett.7b01243

Wang, Y., He, J., Chen, H., Chen, J., Zhu, R., Ma, P., et al. (2016). Ultrastable, Highly Luminescent Organic-Inorganic Perovskite-Polymer Composite Films. *Adv. Mater.* 28, 10710–10717. doi:10.1002/adma.201603964

Wood, V., and Bulović, V. (2010). Colloidal Quantum Dot Light-Emitting Devices. *Nano Rev.* 1, 5202. doi:10.3402/nano.v1i0.5202

Xu, H., Wang, J., Xuan, T., Lv, C., Hou, J., Zhang, L., et al. (2019). Convenient and Large-Scale Synthesis of High-Quality, All-Inorganic lead Halide Perovskite Nanocrystals for white Light-Emitting Diodes. *Chem. Eng. J.* 364, 20–27. doi:10.1016/j.cej.2019.01.152

Xu, Y., Lou, S., Xia, C., Xuan, T., and Li, H. (2020). Controllable Synthesis of All Inorganic lead Halide Perovskite Nanocrystals and white Light-Emitting Diodes Based on $CsPbBr_3$ Nanocrystals. *J. Lumin.* 222, 117132. doi:10.1016/j.jlumin.2020.117132

Xuan, T., Huang, J., Liu, H., Lou, S., Cao, L., Gan, W., et al. (2019). Super-Hydrophobic Cesium Lead Halide Perovskite Quantum Dot-Polymer Composites with High Stability and Luminescent Efficiency for Wide Color Gamut White Light-Emitting Diodes. *Chem. Mater.* 31, 1042–1047. doi:10.1021/acs.chemmater.8b04596

Yan, F., Tan, S. T., Li, X., and Demir, H. V. (2019). Light Generation in Lead Halide Perovskite Nanocrystals: LEDs, Color Converters, Lasers, and Other Applications. *Small* 15, 1902079. doi:10.1002/smll.201902079

Yang, B., Mei, S., He, H., Zhu, Y., Hu, R., Zou, J., et al. (2022). Lead Oxide Enables lead Volatilization Pollution Inhibition and Phase Purity Modulation in Perovskite Quantum Dots Embedded Borosilicate Glass. *J. Eur. Ceram. Soc.* 42, 258–265. doi:10.1016/j.jeurceramsoc.2021.09.052

Yang, M., Peng, H.-s., Zeng, F.-l., Teng, F., Qu, Z., Yang, D., et al. (2018). *In Situ* silica Coating-Directed Synthesis of Orthorhombic Methylammonium lead Bromide Perovskite Quantum Dots with High Stability. *J. Colloid Interf. Sci.* 509, 32–38. doi:10.1016/j.jcis.2017.08.094

Yang, Z., Gao, M., Wu, W., Yang, X., Sun, X. W., Zhang, J., et al. (2019). Recent Advances in Quantum Dot-Based Light-Emitting Devices: Challenges and Possible Solutions. *Mater. Today* 24, 69–93. doi:10.1016/j.mattod.2018.09.002

Zeng, F.-l., Yang, M., Qin, J.-l., Teng, F., Wang, Y.-q., Chen, G.-x., et al. (2018). Ultrastable Luminescent Organic-Inorganic Perovskite Quantum Dots via Surface Engineering: Coordination of Methylammonium Bromide and Covalent Silica Encapsulation. *ACS Appl. Mater. Inter.* 10, 42837–42843. doi:10.1021/acsami.8b14677

Zhang, H., Wang, X., Liao, Q., Xu, Z., Li, H., Zheng, L., et al. (2017). Embedding Perovskite Nanocrystals into a Polymer Matrix for Tunable Luminescence Probes in Cell Imaging. *Adv. Funct. Mater.* 27, 1604382. doi:10.1002/adfm.201604382

Zhang, J., Hodes, G., Jin, Z., and Liu, S. (2019). All-Inorganic $CsPbX_3$ Perovskite Solar Cells: Progress and Prospects. *Angew. Chem. Int. Ed.* 58, 15596–15618. doi:10.1002/anie.201901081

Zhang, Y., Li, G., She, C., Liu, S., Yue, F., Jing, C., et al. (2021). Room Temperature Preparation of Highly Stable Cesium lead Halide Perovskite Nanocrystals by Ligand Modification for white Light-Emitting Diodes. *Nano Res.* 14, 2770–2775. doi:10.1007/s12274-021-3283-5

Zhao, X., Jia, W., Wang, H., Yan, G., Sun, Y., Tang, X., et al. (2022). Preparation of $CH_3NH_3PbBr_3$ Perovskite Quantum Dots Composites with High Photoluminescence Quantum Yield and Good Stability. *J. Lumin.* 245, 118749. doi:10.1016/j.jlumin.2022.118749

Zhao, X., and Park, N.-G. (2015). Stability Issues on Perovskite Solar Cells. *Photonics* 2, 1139–1151. doi:10.3390/photonics2041139

Zheng, Y., Yuan, X., Yang, J., Li, Q., Yang, X., Fan, Y., et al. (2020). Cu Doping-Enhanced Emission Efficiency of Mn^{2+} in Cesium lead Halide Perovskite Nanocrystals for Efficient white Light-Emitting Diodes. *J. Lumin.* 227, 117586. doi:10.1016/j.jlumin.2020.117586

Zhou, Y., and Zhao, Y. (2019). Chemical Stability and Instability of Inorganic Halide Perovskites. *Energ. Environ. Sci.* 12, 1495–1511. doi:10.1039/c8ee03559h

Conflict of Interest: The authors declare that the research was conducted in the absence of any commercial or financial relationships that could be construed as a potential conflict of interest.

Publisher's Note: All claims expressed in this article are solely those of the authors and do not necessarily represent those of their affiliated organizations, or those of the publisher, the editors, and the reviewers. Any product that may be evaluated in this article, or claim that may be made by its manufacturer, is not guaranteed or endorsed by the publisher.